NOAA Technical Memorandum NWS WR-283

Effects of Wildfire in the Mountainous Terrain of Southeast Arizona: Empirical Formulas to Estimate from 1-Year through 10-Year Peak Discharge from Post-Burn Watersheds

William B. Reed[1] and Mike Schaffner[2]
July 2008

[1] NOAA National Weather Service, Colorado Basin River Forecast Center, Salt Lake City
[2] NOAA National Weather Service, Weather Forecast Office, Binghampton, NY

United States Department of Commerce
Carlos M. Gutierrez, Secretary

National Oceanic and Atmospheric Administration
VADM C. Lautenbacher
Under Secretary

National Weather Service
Dr. John (Jack) Hayes, Assistant Administrator for Weather Services

And is approved for publication by
Scientific Services Division
Western Region

Andy Edman, Chief
Scientific Services Division
Salt Lake City, UT

Effects of Wildfire in the Mountainous Terrain of Southeast Arizona: Empirical Formulas to Estimate from 1-Year through 10-Year Peak Discharge from Post-Burn Watersheds

William B. Reed[*] *and Mike Schaffner*[**]
[*]NOAA National Weather Service, Colorado Basin River Forecast Center, Salt Lake City, UT
[**]NOAA National Weather Service, Weather Forecast Office, Binghamton, NY

Abstract. In the desert southwest of the United States, wildfire alters the hydrologic response of watersheds greatly increasing the magnitudes and frequency of flash floods. The NOAA National Weather Service is tasked with the issuance of flash flood warnings to save life and property. Tools that allow the weather forecast offices to quickly access the peak flow magnitude and flood potential from burned areas is highly desirable. The application of readily available topographic and burn severity data make this possible through a series of empirical equations. This paper describes the development of several empirical equations to predict post-burn peak flows expected in response to forecast rainfall events with known return interval. These equations work well for the documented watersheds: the lowest adjusted R-squared value is 0.94. The cornerstone of their predictive usefulness is a multivariate runoff index. The index incorporates four easily determined factors; the sum of high and moderate burn severity area (the hyper-effective drainage area), the average basin elevation, the modified channel relief ratio, and the return interval of forecast rainfall. The new equations predict the runoff from the hyper-effective drainage area. To obtain the runoff from the entire watershed, the runoff from the remaining watershed (calculated using standard methods) is added to the results.

Additional keywords: Arizona; Post-Burn Hydrology; Forest Hydrology; Wildfire; Peak Flows; Flash Floods; Modified Channel Relief Ratio; Hyper-Effective Drainage Area; Multivariate Runoff Index.

Introduction

A multivariate runoff index approach has been developed by Reed and Schaffner (2007) and is utilized here to develop a series of equations to estimate peak discharge from small post-burn watersheds in the semi-arid mountainous terrain of Southeast Arizona for events with return intervals ranging from 1 to 10 years. These equations predict the peak runoff from the hyper-effective drainage area. The hyper-effective drainage area is that portion of the basin that has recently experienced moderate or greater burn severity. To obtain the peak runoff from the entire watershed, the peak from the remaining watershed (calculated using standard methods) is added to the results. As described in Schaffner and Reed (2005a) peak flows from post-burn mountainous terrain may be several orders of magnitude greater than what they would have been for pre-burn conditions. This was observed for various watersheds in the Santa Catalina, Santa Rita, and Pinaleno Mountains.

Six envelope curve and best-fit equation pairs, Equations 2-13, have been developed (see pgs.4-6 and Figures 3-8). For small post-burn watersheds in the semi-arid mountainous terrain of Southeast Arizona, the alternative t-year envelope curve, Equation 12, will provide a conservative estimate of the expected post-burn runoff from the hyper-effective drainage area. This equation provides an estimate of peak flood flow from the hyper-effective drainage area using the return interval of the forecast rainfall event as a variable. Equation 12 will provide a conservative estimate for any return interval of rainfall between 1 and 10 years with a rainfall duration equal to or greater than the basin's time of concentration. The ***time of concentration*** is the time it takes for water to travel from the most distant point of a watershed to the outlet or other point of interest (Chow, 1964).

Data Specifications

Data for the eleven watersheds used in this study are presented in Figures 1 and 2 and are consistent with the data presented in Schaffner and Reed (2005a), Schaffner and Reed (2005b), and Reed and Schaffner (2007). The basic data characteristics are:

- ✓ The event is a short-term thunderstorm with a duration approximately equal to or greater than the time of concentration for the burned basin at outlet[1];
- ✓ The return interval of rainfall is equal to or less than the 10-year return interval;
- ✓ The storm core moved over at least a portion of the hyper-effective drainage area;
- ✓ The documented flood was the "first or second major flush" since watershed burned;
- ✓ The burn occurred in the mountainous terrain of Southeast Arizona; and
- ✓ The basin was uncontrolled (no significant dams or other hydraulic structures).

Empirical Equations

The envelope curve and best-fit equation pairs are presented in Figures 3-8. These equations are for post-burn Southeast Arizona watersheds during recovery. The data used to develop these equations included sites with average basin elevations from 5500 to 8100 feet (1676.4 to 2469 meters) above msl.

Two types of empirical equations were developed:

1) Fixed Flow Return Interval (2-year, 5-year, and 10-year); and
2) Not Assigned Flow Return Interval for 1-10 year events (t-year, with rainfall return interval a variable).

Envelope curves traditionally have been used to define the upper bound of regional flood experience. Therefore the envelope curves here were developed to provide equations that always resulted in values greater than those observed. These curves traditionally have been hand drawn; however, the authors have utilized software to develop these curves by selecting a subset of the data points and then fitting a curve through 1.1 times the values for the selected points. This process was repeated several times until a useful equation was created.

Equations 4 and 5 assign a peak flow return interval of 2-years; Equations 6, 7, 8, and 9 assign a peak flow return interval of 5-years[2]; and Equations 10 and 11 assign a peak flow return interval of 10-years.

The t-year equations are different from the fixed flow return interval equations in that the predicted peak flood flows are not assigned a specific return interval. However, in practice, it appears if the above data specifications are met, the return interval of the flood can be considered equal to the return interval of the rainfall.

[1] To extend the limited dataset from ten to eleven watersheds, Romero Canyon was used although the storm duration was 0.5 hours and the time of concentration was 1.1 hours. It appears that this short duration high intensity 10-year rainfall event may have resulted in a runoff event with a return interval greater than 10 years— using Equation 3 provides an estimate of 12.5 years rather than 10 years. Therefore, the 10-year envelope equation may slightly over estimate runoff. It is interesting that the t-year and 10-year best fit equations do not closely fit Romero Canyon and are therefore essentially unaffected by the use of this data point.

[2] Equations 8 and 9 are from Reed and Schaffner, 2007 and are presented here for comparison. Equations 8 and 9 determine the runoff from the entire basin. Only ten basins (sans Cañada del Oro) were used to develop Equations 8 and 9. Cañada del Oro was not used because of its size. The ten basins included Romero Canyon, with a storm duration less than the time of concentration, to extend the dataset from nine to ten basins. An estimate of the peak flow return interval for Romero Canyon is 12.5 years rather than 10 years (the return interval of the storm).

Multivariate Runoff Index Approach

As described in Reed and Schaffner (2007) the multivariate runoff index utilizes the hyper-effective drainage area (determined from burn severity), average basin elevation, and an objective — southeast Arizona specific — modified channel relief ratio. The ***hyper-effective drainage area*** (variable $\alpha\psi$ in square miles) is the area of the high severity burn plus the area of the moderate severity burn. The ***average basin elevation*** (variable ϕ in thousands of feet) is the average altitude above mean sea level using the elevation of the highest point of the basin and the elevation of the basin outlet. The ***modified channel relief ratio*** (variable β in feet/feet) is the average slope of the basin along the first order channel measured from 1,250 feet (381 meters) below the ridge to the basin outlet. (For the mountain ranges of this study, 1,250 feet below ridge top was used to provide a uniformed estimate of where first order channels begin without the need for further field reconnaissance.) These three variables are intentionally simple to insure the ease and to facilitate the timeliness of equation use. Additionally, the multivariate runoff indexes for Equations 2, 3, 12, and 13 require the ***return interval of the forecast rainfall event*** (variable λ in years). The return interval is determined by taking the lat/long for the basin centroid and utilizing NOAA Atlas 14 (Bonnin, et al, 2004) to determine the return interval of the corresponding rainfall for the location and time frame in question (i.e., utilizing the forecast event's magnitude and duration at the basin of interest centroid)[3].

Previous Method

The previous method developed by Reed and Schaffner (2007) resulted in equations (Equations 8 and 9) that determined the runoff for the entire watershed. This procedure was for small watersheds less than 15 square miles. As shown in Figure 9, the non hyper-effective drainage area contributed 0.2% to 26.4% of the post-burn peak flow. Therefore the contribution was effectively less than or the same as the reported error and could be ignored. These equations are easy to use in that the total peak runoff can be calculated in one step. However, the usefulness of these equations is limited because they are not applicable to larger watersheds.

New Method (Paradigm Shift)

To extend the usefulness of the approach presented here, equations were developed that determined the peak runoff from the hyper-effective drainage area only. To calculate the runoff for the entire watershed, the peak runoff from the remaining watershed must be added to the value calculated for the hyper-effective drainage area. There are several methods for computing runoff from non-burned, non-hyper-effective drainage areas including small ungaged streams, e.g., the new United States Geological Survey (USGS) web-based tool, StreamStats (Kernell, et. al., 2004). For several basins in this report the pre-burn flows were calculated using the National Flood Frequency (NFF) method for Southern Arizona Region 13 (Ries and Crouse, 2002).

The results for the eleven basins are shown in Figure 10 and 11. The runoff from the remaining watershed can be calculated using any standard method. This was accomplished by the authors by multiplying the pre-burn watershed total runoff by the percent of the total watershed that is non hyper-effective after the burn. Although an extra step was introduced, it proved applicable to all eleven watersheds including Cañada del Oro, a watershed greater than 15 square miles.

Additionally for this paper, the t-year equations (Equations 2 and 3) were prepared first (see Figure 3). Then the best-fit equation (Equation 3) was used in the calculation of several data points for the fixed flow return interval equations (Equations 4-7 and 10-11) i.e., the data sets used included the observed data points plus additional data points calculated. All these data sets had 11 data points (see Figures 4, 5, and 7).

As a check for the new equations, the results of the previous 5-year equations were compared with the results of the new method (see Figures 12 and 13). Figure 14 shows the 5-year basin response under burn

[3] For return intervals less than 1 year, 1 year is used.

conditions for the eleven watersheds using the t-year equation, the new 5-year equation, and the previous 5-year equation. Also, for the new method, the basin specific ratio of pre-burn peak flow to post-burn peak flow was calculated for the 2-year, 5-year, and 10-year return intervals using the new best-fit t-year equation (see Figures 15, 16, and 17). The previous method assumed the same ratio for these intervals.

Multivariate Runoff Indexes

The empirical equations use a multivariate runoff index defined as

$$mvi = 1000(\alpha\psi)^a \beta^b \phi^c \lambda^d \quad \textbf{(1)}$$

where

mvi = multivariate runoff index

α = fraction of total watershed with moderate or greater burn severity (square miles/square miles);

ψ = total drainage area (square miles);

β = modified channel relief ratio (feet/feet);

ϕ = average basin elevation above mean sea level (thousands of feet);

λ = recurrence interval of rainfall (t-years); and

a, b, c, and d are respective exponents[4].

Each equation has a slightly different multivariate runoff index form:

multivariate runoff index for 1 to 10 year events (mvi_1) $=1000(\alpha\psi)^{0.51}\beta^{1.91}\phi^{-1.99}\lambda^{0.78}$;

multivariate runoff index for 2-year events (mvi_2) $=1000(\alpha\psi)^{0.48}\beta^{1.78}\phi^{-1.94}$;

multivariate runoff index for 5-year events (mvi_3) $=1000(\alpha\psi)^{0.54}\beta^{1.94}\phi^{-1.98}$;

alternative multivariate runoff index for 5-year events (mvi_4) $=1000(\alpha\psi)^{0.54}\beta^{2}\phi^{-1.28}$;

multivariate runoff index for 10-year events (mvi_5) $=1000(\alpha\psi)^{0.54}\beta^{1.97}\phi^{-2.03}$;

and

alternative multivariate runoff index for 1 to 10 year events (mvi_1) $=1000(\alpha\psi)^{0.51}\beta^{1.91}\phi^{-1.99}\lambda^{0.78}$.

Both t-year equations (for 1 to 10 year events) use the same multivariate runoff index (mvi_1).

T-Year Events (Hyper-Effective Drainage Area Contribution)

The envelope curve equation for 1 to 10 year rainfall events is

$$Q_t = 1870.5(mvi_1) \quad \textbf{(2)}$$

and the corresponding best-fit equation is

$$Q_t = 1422.5(mvi_1)^{0.998} \quad \textbf{(3)}$$

where

Q_t = post-burn runoff for the t-year return interval (cfs).

The R-squared value for the best-fit curve is 0.96. The adjusted R-squared is 0.94. The ***adjusted R-squared*** is a version of the coefficient of determination (R-squared) that has been adjusted to take into account the sample size and the number of predictors in the model. It is an important measure for checking the overall utility of a multiple regression model (Stephens, 2004). It was found that using the recurrence interval of the forecast rainfall (λ) was a slight improvement over using the values for basin average precipitation directly[5].

[4] For the fixed year indexes d= 0 and therefore $\lambda^0 = 1$.

[5] The adjusted R-squared for such an equation is 0.81.

The envelope curve was developed by adding 10% (the upper bound of regional flood experience) to the values for Sabino, Madera, Romero, and Marijilda Canyons; and then fitting a straight line to these data points. A y-intercept of zero was used.

2-Year Events (Hyper-Effective Drainage Area Contribution)

The envelope curve equation for 2-year events is

$$Q_2 = 2026(mvi_2) \quad \textbf{(4)}$$

and the corresponding best-fit equation is

$$Q_2 = 1687.1(mvi_2)^{0.998} \quad \textbf{(5)}$$

where

Q_2 = post-burn runoff for the 2-year return interval (cfs).

The R-squared value for the best-fit curve is 0.97. The adjusted R-squared is 0.96. The envelope curve was developed by adding 10% to the values for Sabino, Deadman, and Marijilda Canyons; and then fitting a straight line to these data points. A y-intercept of zero was used. Hydrologic recovery to near pre-burn conditions takes 3 to 5 years. The 2-year event has a 97% chance of occurring one or more times in 5 years.

5-Year Events (Hyper-Effective Drainage Area Contribution)

The envelope curve equation for 5-year events is

$$Q_5 = -639.7(mvi_3)^2 + 6826(mvi_3) \quad \textbf{(6)}$$

and the corresponding best-fit equation is

$$Q_5 = 5118.7(mvi_3)^{1.002} \quad \textbf{(7)}$$

where

Q_5 = post-burn runoff for the 5-year return interval (cfs).

The R-squared value for the best-fit curve is 0.99. The adjusted R-squared is 0.99. The envelope curve was developed by adding 10% to the values for Madera, Noon, Sabino, and Marijilda Canyons; and then fitting a polynomial to these data points. A y-intercept of zero was used. Hydrologic recovery to near pre-burn conditions takes 3 to 5 years. The 5-year event has a 67% chance of occurring one or more times in 5 years.

Alternative Equation 5-Year Events (Previously Published: Entire Watershed)

The envelope curve equation for 5-year events is

$$Q_5 = 4114(mvi_4)^{0.65} \quad \textbf{(8)}$$

and the corresponding best-fit equation is

$$Q_5 = 1993(mvi_4) \quad \textbf{(9)}$$

where

Q_5 = post-burn runoff for the 5-year return interval (cfs).

The R-squared value for the best-fit curve is 0.97. The adjusted R-squared is 0.96. The envelope curve was developed by adding 25% (the largest reported flow measurement error) to the values for Deadman, Romero, and Marijilda Canyons; and then fitting a power curve to these data points. A power function was used to insure the curve went through the origin, (0,0). Hydrologic recovery to near pre-burn conditions takes 3 to 5 years. The 5-year event has a 67% chance of occurring one or more times in 5 years.

As described in Reed and Schaffner (2007) on page 9, the leave-one-out cross validation technique was used to test this equation ability to predict Q5 for the entire watershed. This validation technique allows each data point to be treated, one at a time, as independent data (Wilks, 2006). Using this process, a cross validation adjusted R-square value of 0.81 was obtained with a corresponding cross validation standard error of 1757 cfs

(49.8 cubic meters per second). This yields a cross validation adjusted coefficient of determination (adjusted correlation coefficient) of 0.90.

10-Year Events (Hyper-Effective Drainage Area Contribution)

The envelope curve equation for 10-year events is

$$Q_{10} = -2269.3(mvi_5)^2 + 14329(mvi_5) \quad \textbf{(10)}$$

and the corresponding best-fit equation is

$$Q_{10} = 10223(mvi_5) \quad \textbf{(11)}$$

where

Q_{10} = post-burn runoff for the 10-year return interval (cfs).

The R-squared value for the best-fit curve is 0.99. The adjusted R-squared is 0.99. The envelope curve was developed by adding 10% to the values for Noon, Sabino, Campo Bonito, and Romero Canyons; and then fitting a polynomial to these data points. A y-intercept of zero was used. Hydrologic recovery to near pre-burn conditions takes 3 to 5 years. The 10-year event has a 41% chance of occurring one or more times in 5 years.

Alternative Equation T-Year Events (Hyper-Effective Drainage Area Contribution)

The alternative equation for 1 to 10 year rainfall events was developed using the four previous datasets (37 data points) combined in an attempt to merge the two types of equations. Both t-year equations (for 1 to 10 year events) use the same multivariate runoff index (mvi_1). The resulting envelope curve equation is

$$Q_t = -55.819(mvi_1)^2 + 2138.9(mvi_1) \quad \textbf{(12)}$$

and the alternative best-fit equation is

$$Q_t = 1422.5(mvi_1)^{0.998} \quad \textbf{(13)}$$

where

Q_t = post-burn runoff for the t-year return interval (cfs).

The R-squared value for the best-fit curve is 0.99. The adjusted R-squared is 0.99. The envelope curve was developed by adding 10% to the values for 6 of the 37 data points; and then fitting a polynomial to these points. A y-intercept of zero was used. As would be expected, the best fit t-year equations, Equation 3 and Equation 13, are the same.

Comparison of Envelope Equations

- For a comparison of envelope equations (Equations 2, 4, 6, and 10) for hyper-effective drainage area's peak flow contribution see Figure 18. The fixed-year equations result in values slightly greater than the corresponding t-year equation values.

- For a comparison of the two t-year envelope curves (Equations 2 and 12) for hyper-effective drainage area's peak flow contribution see Figure 19. The two curves provide essentially the same results for the basins with hyper-effective drainage area peak flows less than 11500 cfs. For the basin with peak flows greater than 11500 cfs, Envelope Curve 12 provides the lower values.

- For a total runoff comparison of fixed-year envelope curves for 5-year post-burn events see Figure 12. The new envelope curve is always less than previous envelope curve.

Comparison of Best-Fit Equations

- For a comparison of best fit equations (Equations 3, 5, 7, and 11) for hyper-effective drainage area's peak flow contributions see Figure 20. The fixed-year equations and the t-year equation result in essentially the same values.

- The two t-year best fit equations (Equations 3 and 13) for hyper-effective drainage area's peak flow contribution are the same.

- For a total runoff comparison of best fit equations for the 5-year post-burn events see Figure 13. Curves are essentially the same for four data points (Alder, Campo Bonito, Romero, and Sabino Canyons). The new best fit curve is less than previous best fit curve for the other 6 data points.

Comparison of 10-Year Envelope Curve (Equation 10) Results and Maximum Flood Flow

- For a comparison of the results of the new 10-year envelope curve (Equation 10) with the results for maximum flood flow calculated using the method presented in Crippen and Bue (1977) see Figure 21. All Envelope Curve values are below the corresponding maximum flood flows. However, the 10-year values for Noon and Wet Canyons approach maximum flood flow.

Comparison of T-Year Envelope Curve (Equation 12) Results and Maximum Flood Flow

- For a comparison of the results of alternative t-year envelope curve (Equation 12) using a return interval of 10 years with the results for maximum flood flow calculated using the method presented in Crippen and Bue (1977) see Figure 22. All Envelope Curve values are below the corresponding maximum flood flows. However, the 10-year values for Noon and Wet Canyons approach maximum flood flows.

Basin Specific Pre-Burn to Post-Burn Ratios

- The previous method assumed the same ratio of pre-burn peak flow to post-burn peak flow for the 2-year, 5-year, and 10-year return intervals. Using the new best-fit t-year equation, the basin specific ratio of pre-burn peak flow to post-burn peak flow were calculated for the 2-year, 5-year, and 10-year return intervals (see Figures 15, 16, and 17). The watersheds can be broken out into two groups:
  1) The Pinaleno Mountain basin specific total watershed post-burn to pre-burn peak flow ratios are all above 10 and the ratios decrease as return interval increases (Figure 15).
  2) The Santa Rita and Catalina Mountains basin specific total watershed post-burn to pre-burn peak flow ratios are all below 10 (Figure 17). These adjusted ratios were calculated using the t-year best fit equation and slightly increasing the results of the 5-year values — the values were increased 10% to 15.5%. Such an increase is within the reported error of 25%. In general, the values decrease as the return interval increases. Unadjusted results are presented in Figure 16.

Discussion

The new method (equations 2-7, and equations 10-13) requires a new step: calculating the peak flow from the remaining watershed (the non hyper-effective watershed). The use of the new equations calculates only the peak flow for the hyper-effective drainage area. Two examples of the use of these equations (and

where appropriate the previous method) are provided in Appendix I. The advantage to the new method is that it can be applied to larger watersheds (previous method was limited to watershed smaller than 15 square miles).

The use of the new equations result in different basin specific ratios of pre-burn to post-burn peak flows for different return intervals. In general, the ratios decrease as the return interval increases. The authors believe this is more representative of expected basin response in that as the return interval increases the sheer volume of water overwhelms any effect of hydrophobic soils and other burn related conditions such as temporary damming. Additionally the different ratios for the 5-year events calculated using the different methods still indicate that the post-burn response of watersheds in the mountainous terrain of southeast Arizona can be hundred of times greater than the response under normal (pre-burn) conditions.

Whereas the t-year and fixed year equations provide similar results, the alternative t-year envelope curve, Equation 12, consistently provides reasonable results across the full range of observed peak flows. These results, as designed, are always above the observed values; and provide a conservative estimate of peak flows.

The envelope curve for the 10-year return interval (Equation 10) provides results less than the basins' maximum peak flow values calculated using the Crippen and Bue method. As expected this indicates that the maximum values would likely result from larger storms[6] (storms with return intervals greater than 10 years).

Conclusions

- The multivariate runoff index approach is a useful technique for evaluating the peak flow response from post-burn watersheds during recovery.

- The hyper-effective drainage area is responsible for a major portion of the increase in peak flows.

- Peak flows during recovery can be up to 107.6 times greater than under pre-burn conditions.

- The new method with slight modifications may be applicable to other regions of the Southwestern United States in that it is not limited to small watersheds. The steps are presented in Appendix III.

- Two types of equations for determining Post-Burn Peak Flows have been developed:
    1) Fixed Flow Return Interval (2-Year, 5-Year, and 10-Year Equations); and
    2) Rainfall Return Interval a Variable and Flow Return Interval Not Assigned (T-Year Equations).

- The alternative t-year envelope curve, Equation 12, is suggested for most applications.

[6] Using Equation 3 for the documented post-burn conditions, the maximum peak flow during recovery:
for Noon and Wet Canyons may occur from a storm as small as the 25-year event;
for Deadman Canyon may occur from a storm as small as the 50-year event;
for Frye, Madera, and Marijila Canyons may occur from a storm about the 75-year event;
for Campo Bonito and Romero Canyons may occur from a storm about the 100-year event: and
for Alder, Cañada del Oro, and Sabino Canyons may occur from a storm about the 500-year event.
Alder, Cañada del Oro, and Sabino Canyons have the smallest basin specific total watershed post-burn to pre-burn peak flow ratios (see Figure 17). Under post-burn conditions the Pinaleno and Santa Rita Mountains appear more likely to experience maximum peak flows than the Santa Catalina Mountains.

Acknowledgements

The authors thank Chris Smith, Dan Evans, and Saeid Tadayon of the U.S. Geological Survey for conducting a slope-area measurement of Marijilda Canyon, their sound advice, and field assistance; thank Barry Scott of Arizona Division of Emergency Management for the GIS analysis of the various watersheds in the Pinaleno Mountains and Santa Catalina Mountains; thank Robert Lefevre of U.S. Forest Service for providing burn severity shapefiles for the Nuttall Fire and burn severity estimates for the Sabino Creek near Mount Lemmon watershed; thank Ann Youberg of the Arizona Geological Survey for providing a HEC-RAS step backwater model analysis for Romero Canyon; and thank Chad Kahler, Service Hydrologist, Tucson WFO for providing additional data for Cañada del Oro. The authors thank Brian McInerney, Senior Service Hydrologist, Salt Lake City WFO for his review of this paper. The authors also thank Jay Breidenbach, Senior Service Hydrologist, Boise WFO for his review of this paper that provided excellent suggestions for improving its readability.

References

Bonnin, G. M., D. Todd, B. Lin, T. Parzybok, M. Yekta, and D. Riley, 2004. Precipitation-Frequency Atlas of the United States, Volume 1: Semiarid Southwest (Arizona, Southeast California, Nevada, New Mexico, Utah). NOAA Atlas 14. Available online: http://hdsc.nws.noaa.gov/hdsc/pfds/pfds_docs.html#volume1.

Chow, V., 1964. Handbook of Applied Hydrology. McGraw-Hill.

Crippen, J. and C. Bue, 1977. Maximum Flood flows in the Conterminous United States. USGS Water Supply Paper 1887.

Kernell G. Ries III, Peter A. Steeves, Jaqueline D. Coles, Alan H. Rea, and David W. Stewart, 2004. StreamStats: A U.S. Geological Survey Web Application for Stream Information. USGS Fact Sheet FS 2004-3115. Available online:
http://md.water.usgs.gov/publications/fs-2004-3115/fs20043115.pdf
Also see:
http://water.usgs.gov/osw/streamstats/index.html

Reed, W. and M. Schaffner, 2007. Effects of Wildfire in the Mountainous Terrain of Southeast Arizona: An Empirical Formula to Estimate 5-Year Peak Discharge from Small Post-Burn Watersheds. NOAA Technical Memorandum NWS WR-279. Available online:
http://www.wrh.noaa.gov/wrh/techMemos/TM-279.pdf.

Ries, K.G., III, and M. Y. Crouse, 2002. The National Flood Frequency Program, Version 3: A Computer Program for Estimating Magnitude and Frequency of Floods for Ungaged Sites, 2002: U.S. Geological Survey Water-Resources Investigations Report 02-4168, 42 p. Available online:
http://pubs.usgs.gov/wri/wri024168/.

Schaffner, M. and W. Reed, 2005a. Effects of Wildfire in the Mountainous Terrain of Southeast Arizona: Post-Burn Hydrologic Response of Nine Watersheds. NOAA National Weather Service Western Region Technical Attachment 05-01. Available online:
http://www.wrh.noaa.gov/wrh/05TAs/ta0501.pdf.

Schaffner, M. and W. Reed, 2005b. Evaluation of Post-Burn Hydrologic Recovery of a Small Mountainous Watershed: Upper Campo Bonito Wash in Southern Arizona. NOAA National Weather Service Western Region Technical Attachment 05-06. Available online:
http://www.wrh.noaa.gov/wrh/05TAs/ta0506.pdf.

Stephens, L., 2004. Advanced Statistics Demystified. McGraw-Hill Professional.

Wilks, D., 2006. Statistical Methods in the Atmospheric Sciences. Academic Press (Elsevier).

APPENDIX I - TWO EXAMPLES

Example One: Calculating the 5-Year Post-Burn Peak Flow for Marijilda Canyon using the appropriate Best Fit Equations: Equations 3, 7, 9, and 13.

Equation 3 is $Q_t = 1422.5(mvi_1)^{0.998}$, Equation 7 is $Q_5 = 5118.7(mvi_3)^{1.002}$, Equation 9 is $Q_5 = 1993(mvi_4)$, and Equation 13 is $Q_t = 1422.5(mvi_1)^{0.998}$; where:

$(mvi_{1)} = 1000(\alpha\psi)^{0.51}\beta^{1.91}\phi^{-1.99}\lambda^{0.78}$, $(mvi_3) = 1000(\alpha\psi)^{0.54}\beta^{1.94}\phi^{-1.98}$, and $(mvi_4) = 1000(\alpha\psi)^{0.54}\beta^{2}\phi^{-1.28}$.

From Figure 2, we see that for Marijilda Canyon: $\alpha\psi$ = 0.59 * 11 = 6.49 square miles, β = 0.15 feet/feet, and ϕ = 7.1 feet/1000. Since we are interested in the 5-year return interval peak flow λ = 5 years. Using these values $\boldsymbol{mvi_1}$ = 1000 times $(6.49)^{0.51}$ times $(0.15)^{1.91}$ times $(7.1)^{-1.99}$ times $(5)^{0.78}$ = 1000 times 2.5960 times 0.0265 times 0.0201 times 3.5091 = **4.85**. Using these values $\boldsymbol{mvi_3}$ = 1000 times 2.745 times 0.02502 times 0.02051 = **1.41**. Using these values $\boldsymbol{mvi_4}$ = 1000 times 2.745 times 0.02233 times 0.0810 = **4.96**.

Step 1: The Result of Equation 3 is 6877 cfs, the result of Equation 7 is 7222 cfs and the result of Equation 13 is the same as Equation 3, 6877 cfs. Step 2: For Equations 3, 7, and 13 we also need to calculate the peak flow from the remaining watershed and add that value to the results of Step 1. From Figure 9 we see that the 5-year pre-burn peak flow for the entire watershed is 313 cfs and that the remaining watershed is 41 % of the watershed, i.e., 1 - 0.59 = 0.41. Therefore the contribution for this portion is 128 cfs, i.e., 0.41 * 313 = 128. Therefore, we have 7005[√] cfs, 7350 cfs, and 7005 cfs for Equations 3, 7, and 13 respectively.

Since the total basin is less than 15 square miles we can use Equation 9. The result of Equation 9 (a one step process) is 9885 cfs.

From Figure 1 we can see that the USGS indirect measurement for Marijilda Canyon peak flow was 8470 cfs and the event was a 5-year event. This illustrates the need to use the envelope curve rather the best fit curve if one wants to be certain of the results being equal to or greater than the observed values. However, we can also see that the best fit Equation 9 overestimates in this case. From Figure 6 we can see that this would occur for only 4 of the 10 basins. Therefore, one would have to use the envelope curve rather the best fit curve if one wants to be certain of the results being equal to or greater than the observed values. Indeed the authors suggest that the alternative t-year envelope curve, Equation 12, be used for most applications.

Figure 10 provides the total peak flow for all eleven basins for 2-year, 5-year, and 10-year return intervals using equation 3. Figure 11 provides the total peak flow for all eleven basins for 2-year, 5-year, and 10-year return intervals using Equation 12.

[√] The value you obtain may be slightly different depending upon how many decimal places you carry in your spreadsheet or calculator. This value is also shown as 7009 in Figure 10, both values are correct. The above was calculated on a calculator, Figure 10 values were calculated in a spreadsheet.

Example Two: Calculating the 2-Year Post Burn Peak Flow for Cañada del Oro using the appropriate Envelope Equations: Equations 2, 4, and 12.

Equation 2 is $Q_t = 1870.5(mvi_1)$, Equation 4 is $Q_2 = 2026(mvi_2)$,
and Equation 12 is $Q_t = -55.819(mvi_1)^2 + 2138.9(mvi_1)$; where:
$(mvi_1)=1000(\alpha\psi)^{0.51}\beta^{1.91}\phi^{-1.99}\lambda^{0.78}$, and $(mvi_2) = 1000(\alpha\psi)^{0.48}\beta^{1.78}\phi^{-1.94}$.

From Figure 2, we see that for Cañada del Oro: $\alpha\psi$ = 0.75 * 21.6 = 16.2 square miles, β = 0.07 feet/feet, and ϕ = 6.8 feet/1000. Since we are interested in the 2-year return interval peak flow λ = 2 years. Using these values $\boldsymbol{mvi_1}$ = 1000 times $(16.2)^{0.51}$ times $(0.07)^{1.91}$ times $(6.8)^{-1.99}$ times $(2)^{0.78}$ = 1000 times 4.1386 times 0.0062 times 0.0221 times 1.717 = **0.97**. Using these values $\boldsymbol{mvi_2}$ = 1000 times 3.807 times 0.008796 times 0.024339 = **0.81**.

Step 1: The Result of Equation 2 is 1814 cfs, the result of Equation 4 is 1641 cfs, and the result of Equation 12 is 2022 cfs. Step 2: For Equations 2, 4, and 12 we also need to calculate the peak flow from the remaining watershed and add that value to the results of Step 1. From Figure 10 we see that the 2-year pre-burn peak flow for the entire watershed is 230 cfs and from Figure 9 we can see that the remaining watershed is 25 % of the watershed, i.e., 1 - 0.75 = 0.25. Therefore the contribution for this portion is 58 cfs, i.e., 0.25 * 230 = 58. Therefore, we have 1872 cfs, 1699 cfs, and 2080[√] cfs for Equations 2, 4, and 12 respectively.

From Figure 1 we can see that the peak flow for Cañada del Oro was 1450 cfs and the event was a 2-year event. This peak was measured by a Pima County Flood Control ALERT stream gauge located on Cañada del Oro near Coronado Camp. Figure 11 provides the total peak flow for all eleven basins for 2-year, 5-year, and 10-year return intervals using Equation 12.

[√] The value you obtain may be slightly different depending upon how many decimal places you carry in your spreadsheet or calculator. This value is also shown as 2096 in Figure 11, both values are correct. The above was calculated on a calculator, Figure 10 values were calculated in a spreadsheet.

APPENDIX II – FIGURES

- **Figure 1:** Southeast Arizona post-burn flood database for eleven basins.
- **Figure 2:** Additional selected basin values for study watersheds in the Pinaleno, Santa Catalina, and Santa Rita Mountains.
- **Figure 3:** An empirical formula for when you know the forecast return interval of the rainfall, specifically to calculate the hyper-effective drainage area contribution.
- **Figure 4:** An empirical equation to estimate post-burn runoff from 2-year rainfall events during recovery (Southeast Arizona Watersheds), specifically to calculate the hyper-effective drainage area contribution.
- **Figure 5:** An empirical equation to estimate 5-year post-burn runoff during recovery (Southeast Arizona Watersheds), specifically to calculate the hyper-effective drainage area contribution.
- **Figure 6:** An empirical equation to estimate 5-year post-burn runoff during recovery (Southeast Arizona Watersheds), specifically to calculate the runoff from the entire drainage area.
- **Figure 7:** An empirical equation to estimate post-burn runoff from 10-year rainfall events during recovery (Southeast Arizona Watersheds), specifically to calculate the hyper-effective drainage area contribution.
- **Figure 8:** An empirical formula for when you know the forecast return interval of the rainfall developed using the four previous datasets combined (37 data points).
- **Figure 9:** Percent of total post-burn peak flow contributed by <u>non</u> hyper-effective drainage area.
- **Figure 10:** Total Watershed Pre-Burn and Post-Burn Peak Flows for 2-Year, 5-Year, and 10-Year Return Intervals using Equation 3.
- **Figure 11:** Total Watershed Pre-Burn and Post-Burn Peak Flows for 2-Year, 5-Year, and 10-Year Return Intervals using Equation 12.
- **Figure 12:** Comparisons of Fixed-Year Envelope Curves for 5-Year Post-Burn Events.
- **Figure 13:** Comparison of Best Fit Equations for the for 5-Year Post-Burn Events.
- **Figure 14:** The 5-Year total watershed peak flow basin response under burn conditions for various watersheds in the Santa Catalina (Sabino, Alder, Campo Bonito, Romero, and Cañada del Oro), Santa Rita (Madera), and Pinaleno Mountains (Marijilda, Frye, Deadman, Noon, and Wet).
- **Figure 15:** The Pinaleno Mountain basin specific total watershed post-burn to pre-burn peak flow ratios for return intervals 2, 5, and 10 years.
- **Figure 16:** The Santa Rita and Catalina Mountains basin specific total watershed post-burn to pre-burn peak flow ratios for return intervals 2, 5, and 10 years.
- **Figure 17:** The Santa Rita and Catalina Mountains basin specific total watershed post-burn to pre-burn peak flow ratios for return intervals 2, 5, and 10 years.
- **Figure 18:** Comparison of Envelope Equations for Hyper-Effective Drainage Area Peak Flow (cfs) Contribution.
- **Figure 19:** Comparison the Two T-Year Envelope Equations for Hyper-Effective Drainage Area Peak Flow (cfs) Contribution.
- **Figure 20:** Comparison of Best Fit Equations for Hyper-Effective Drainage Area Peak Flow (cfs) Contribution.
- **Figure 21:** Comparison of the results of Envelope Curve for the 10-year return interval with the results for maximum flood flow calculated using the method presented in Crippen and Bue (1977).

- **Figure 22:** Comparison of the results of Alternative T-Year Envelope Curve (Equation 12) using a return interval of 10 years and adding the peak for the remaining watershed with the results for maximum flood flow calculated using the method presented in Crippen and Bue (1977).

SOUTHEAST ARIZONA POST-BURN FLOOD DATABASE FOR ELEVEN BASINS							
Watershed	Basin Average Precipitation (inches)	Storm Duration (hours)	General Storm Motion	Time of Concentration (hours)	Rainfall Return Interval (t-years)	Peak Flow of Flood (cfs)	Pre-Burn Peak Flow of Rainfall Return Interval (cfs)
Frye Creek	0.40	0.5	across	0.6	< 1-year	1400[#]	18.5
Deadman Canyon	1.00	0.5	across	0.5	3-year	5500	67.2
Marijilda Canyon	1.25	0.7	across	0.8	5-year	8470[♦]	313
Noon Creek	0.94	0.4	across	0.4	2-year	2684	19
Wet Canyon	0.8	0.7	across	0.3	1-year	1490	7.2
Upper Campo Bonito	1.51	0.5	stationary	0.3	10-year	1900	586
Sabino Creek near Mount Lemmon	1.25	1	stationary	0.6	2-year	350	119
Alder Canyon at Ventana Windmill	1.60	1	down to up	1.2	5-year	3103	1260
Madera Canyon	0.70	0.75	stationary	0.4	< 1-year	1526	224
Romero Canyon	1.60	0.5	up to down	1.1	10-year	9500	1420
Cañada del Oro	1.14	1	up to down	1.3	2-year	1450	230

Figure 1: Southeast Arizona post-burn flood database for eleven basins.

[#] July 27, 2004.

[♦] Value updated based upon October 6, 2004 written communication from USGS (Tadayon, 2004) providing a new peak flow estimate for the flood of August 17, 2004.

ADDITIONAL SELECTED BASIN VALUES					
Watershed	Location	Modified channel relief ratio (ft/ft)	High severity burn + Moderate severity burn (%)	Average basin elevation above mean sea level (ft/1000)	Drainage area (sq mi)
Frye Creek	Pinaleno Mountains	0.19	61	8.1	4.02
Deadman Canyon	Pinaleno Mountains	0.22	51	7.7	4.78
Marijilda Canyon	Pinaleno Mountains	0.15	59	7.1	11
Noon Creek	Pinaleno Mountains	0.24	77	7.7	2.99
Wet Canyon	Pinaleno Mountains	0.26	44	8.1	1.58
Upper Campo Bonito	Santa Catalina Mountains	0.07	80	5.5	1.5
Sabino Creek near Mount Lemmon	Santa Catalina Mountains	0.07	55	8.2	3.4
Alder Canyon at Ventana Windmill	Santa Catalina Mountains	0.08	35	6.1	14
Madera Canyon	Santa Rita Mountains	0.22	15	7.2	4
Romero Canyon	Santa Catalina Mountains	0.12	34	5.7	7.25
Cañada del Oro	Santa Catalina Mountains	0.07[√]	75	6.8[√]	21.6

Figure 2: Additional selected basin values for study watersheds in the Pinaleno, Santa Catalina, and Santa Rita Mountains.

[√] personal communication from Chad Kahler, Service Hydrologist, Tucson WFO on 11/14/2007.

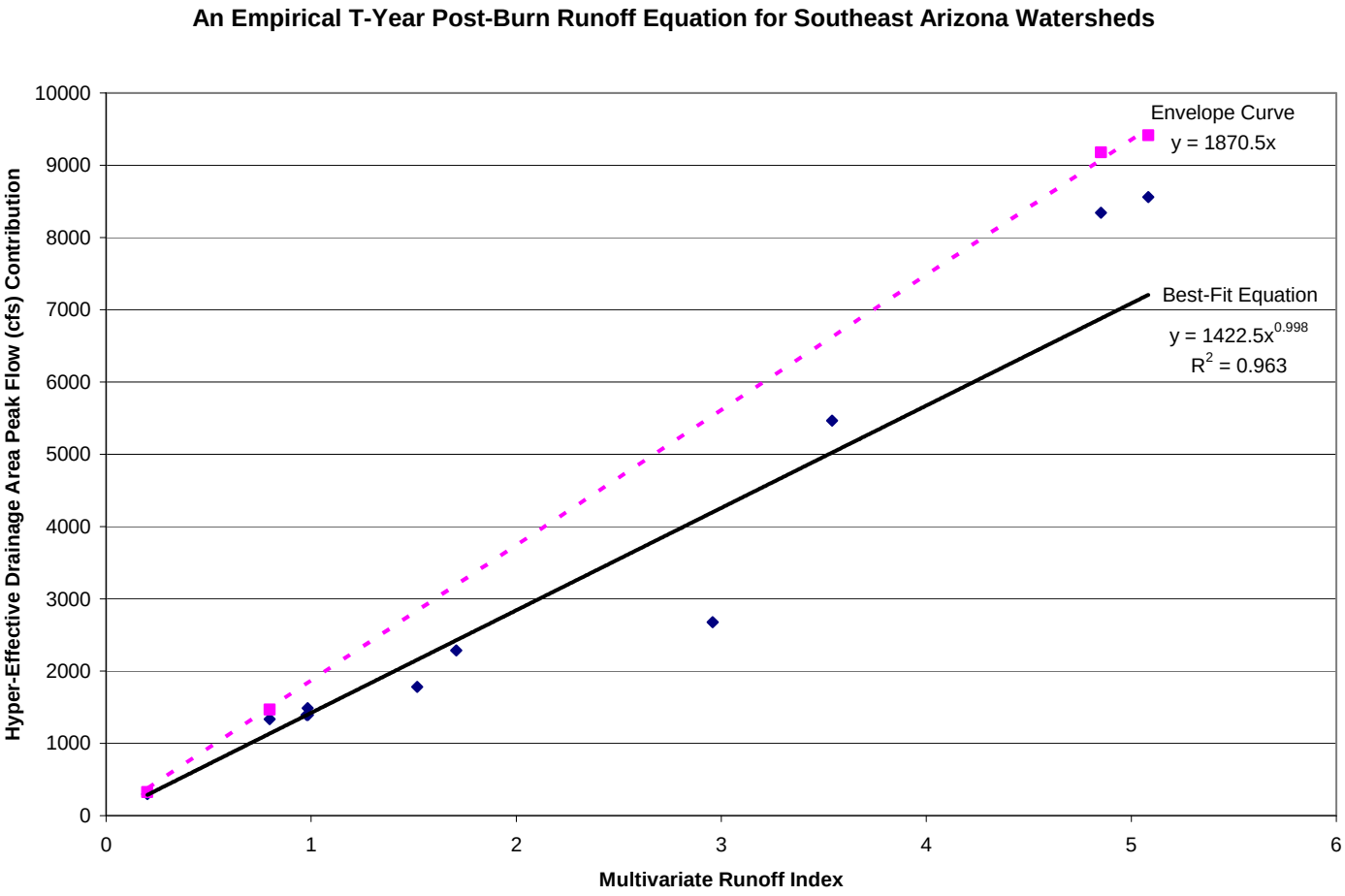

Figure 3: An empirical formula for when you know the forecast return interval of the rainfall, specifically to calculate the hyper-effective drainage area contribution. The best-fit equation and the envelope curve are both essentially straight lines with y-intercepts of zero. Multivariate runoff index $=1000(\alpha\psi)^{0.51}\beta^{1.91}\phi^{-1.99}\lambda^{0.78}$; where α = high severity burn + moderate severity burn as a fraction of total watershed (square miles/square miles); ψ = total drainage area (square miles); β = modified channel relief ratio (feet/feet); ϕ = average basin elevation above mean sea level (thousands of feet) and λ = recurrence interval of rainfall (t-years). Note: α times ψ in above equation = hyper-effective drainage area.

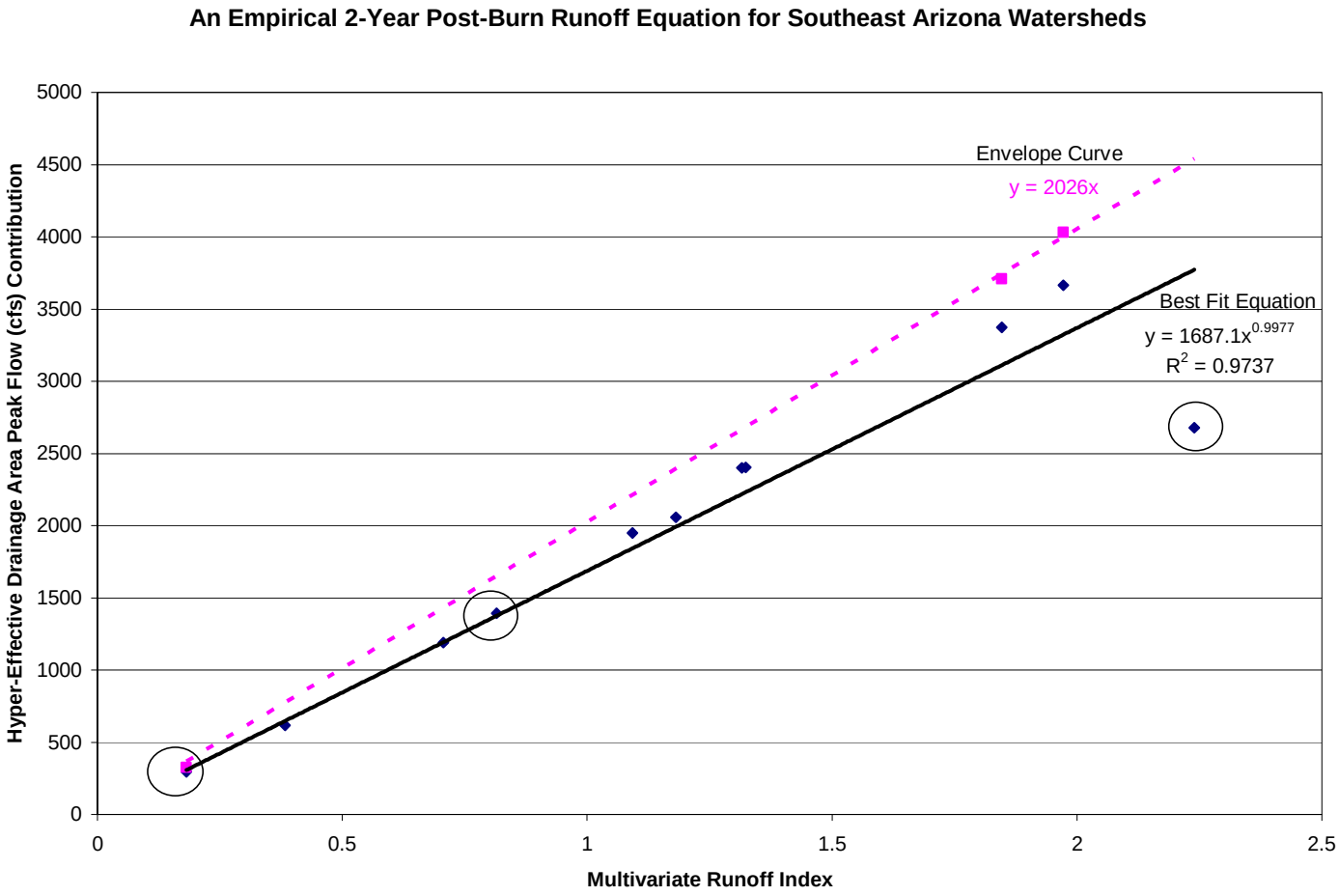

Figure 4: An empirical equation to estimate post-burn runoff from 2-year rainfall events during recovery (Southeast Arizona Watersheds), specifically to calculate the hyper-effective drainage area contribution. The best-fit equation is essentially a straight line with a y-intercept of zero. Multivariate runoff index $=1000(\alpha\psi)^{0.48}\beta^{1.78}\phi^{-1.94}$; where α = high severity burn + moderate severity burn as a fraction of total watershed (square miles/square miles); ψ = total drainage area (square miles); β = modified channel relief ratio (feet/feet); and ϕ = average basin elevation above mean sea level (thousands of feet). Note: α times ψ in above equation = hyper-effective drainage area. The points circled were 2-year events in the database (see Figure 1). The other 8 points were calculated using the other 8 sites in the database and the t-year equation with a storm return interval of 2 years.

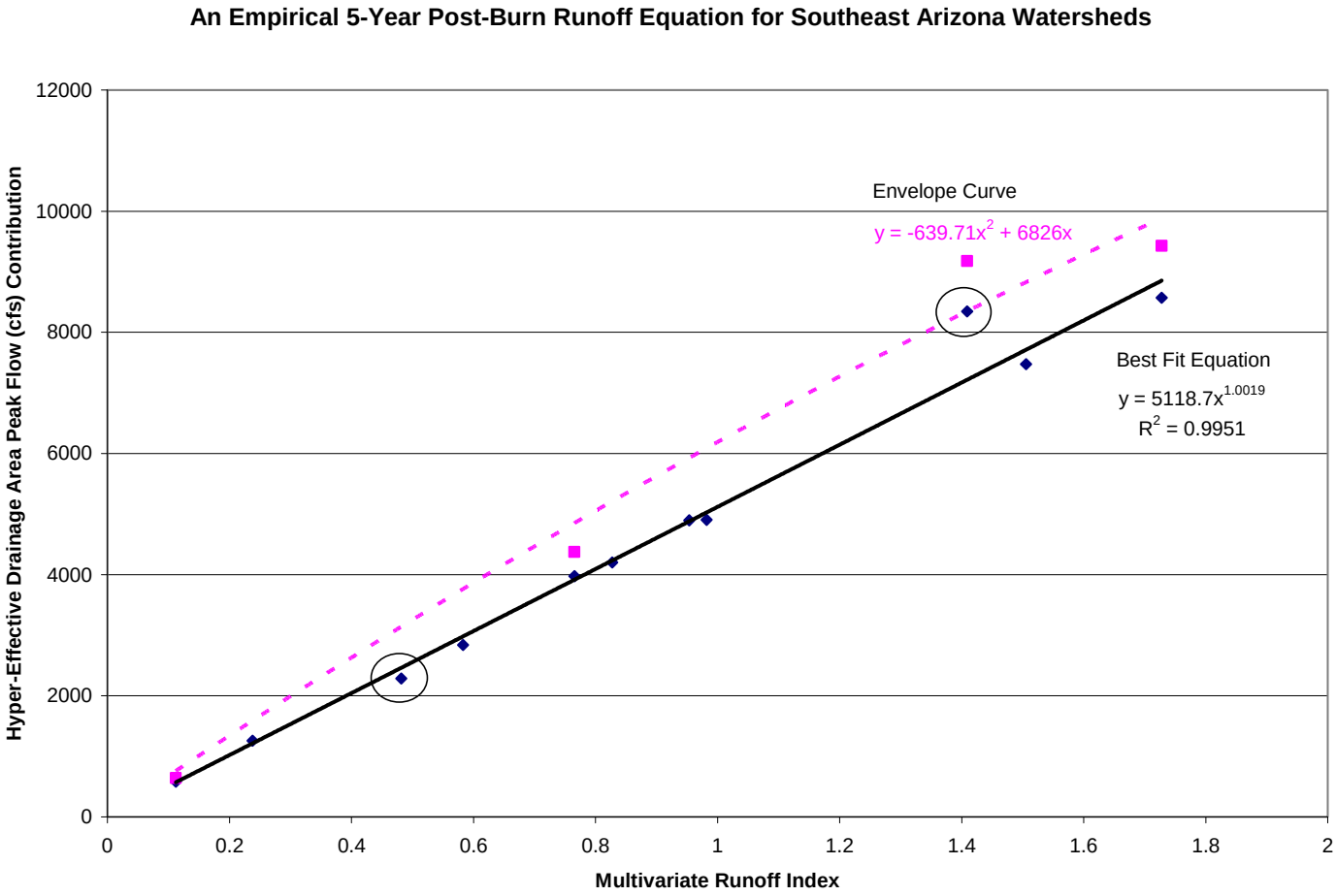

Figure 5: An empirical equation to estimate 5-year post-burn runoff during recovery (Southeast Arizona Watersheds), specifically to calculate the hyper-effective drainage area contribution. The best-fit equation is essentially a straight line with a y-intercept of zero. Multivariate runoff index $=1000(\alpha\psi)^{.054}\beta^{1.94}\phi^{-1.98}$; where α = high severity burn + moderate severity burn as a fraction of total watershed (square miles/square miles); ψ = total drainage area (square miles); β = modified channel relief ratio (feet/feet); and ϕ = average basin elevation above mean sea level (thousands of feet). Note: α times ψ in above equation = hyper-effective drainage area. The points circled were 5-year events in the database (see Figure 1). The other 8 points were calculated using the other 8 sites in the database and the t-year equation with a storm return interval of 5 years.

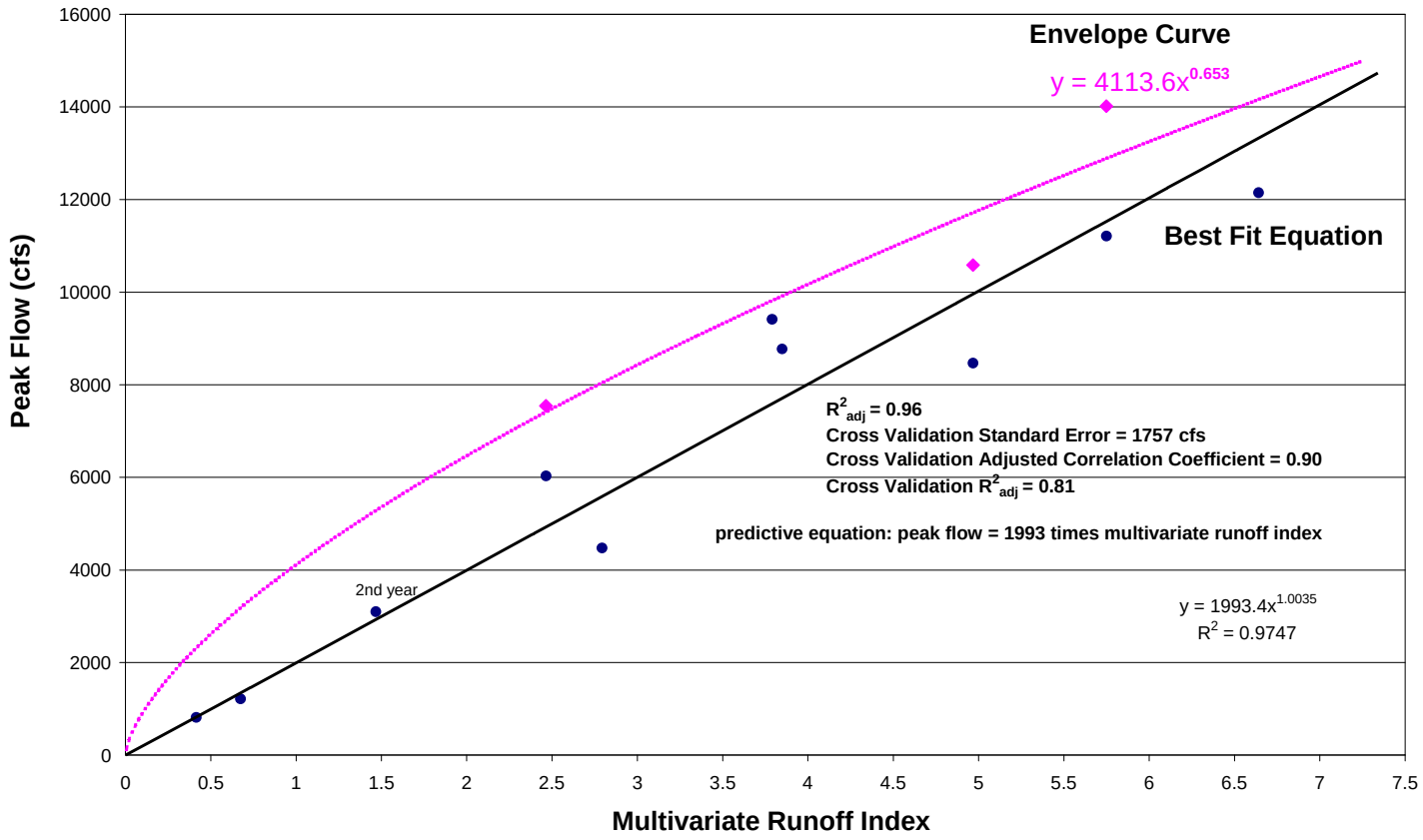

Figure 6: An empirical equation to estimate 5-year post-burn runoff during recovery (Southeast Arizona Watersheds), specifically to calculate the runoff from the entire drainage area. This equation is from Reed and Schaffner (2007) and uses the data of only ten basins. The best-fit equation is essentially a straight line with a y-intercept of zero. 2nd year = those events that occurred during the second year after the burn; the other 9 events occurred during the first year after the burn. Multivariate runoff index $=1000(\alpha\psi)^{0.54}\beta^{2}\phi^{-1.28}$; where α = high severity burn + moderate severity burn as a fraction of total watershed (square miles/square miles); ψ = total drainage area (square miles); β = modified channel relief ratio (feet/feet); and ϕ = average basin elevation above mean sea level (thousands of feet). Note: α times ψ in above equation = hyper-effective drainage area.

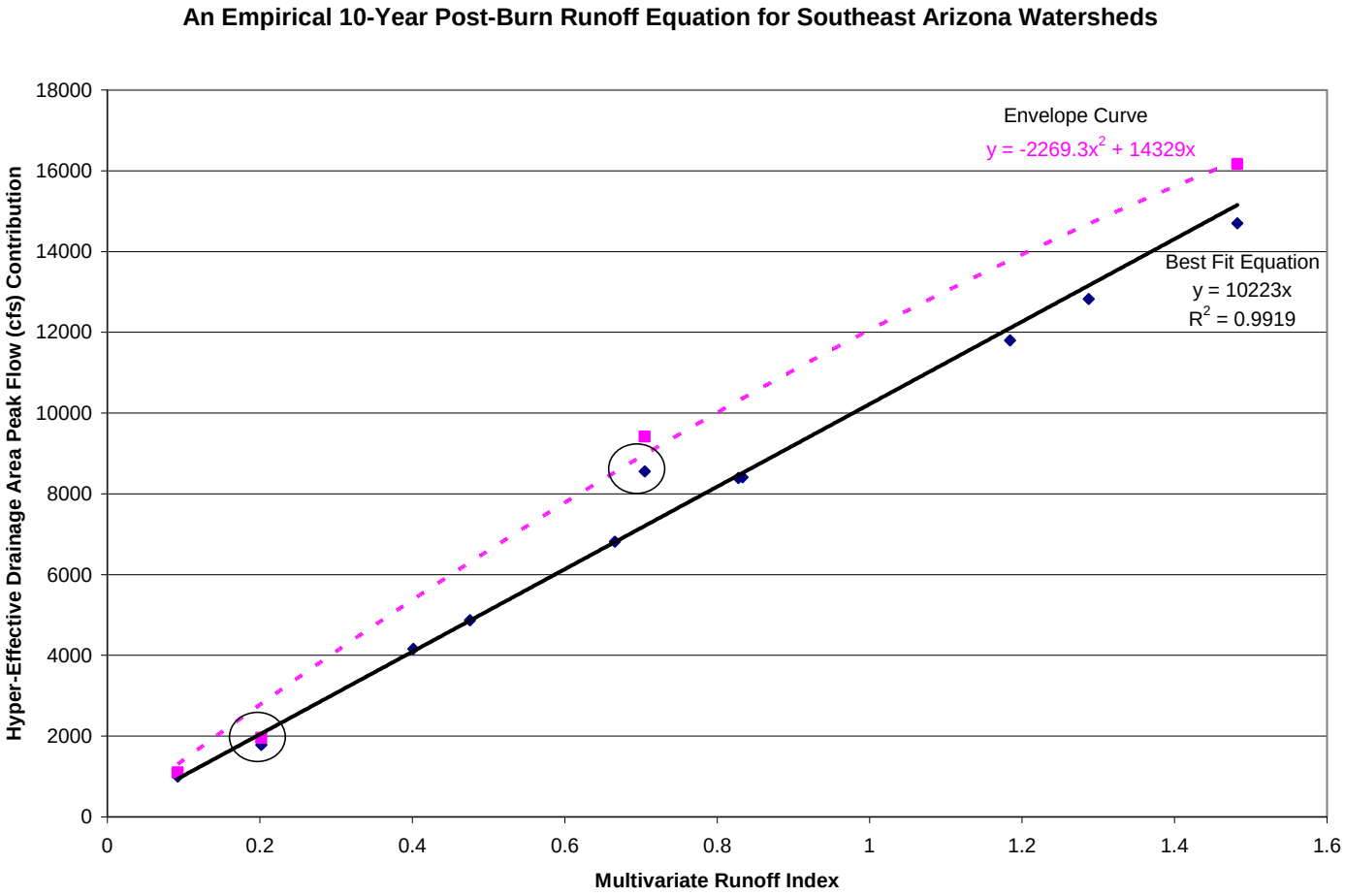

Figure 7: An empirical equation to estimate post-burn runoff from 10-year rainfall events during recovery (Southeast Arizona Watersheds), specifically to calculate the hyper-effective drainage area contribution. The best-fit equation is essentially a straight line with a y-intercept of zero. Multivariate runoff index $=1000(\alpha\psi)^{0.54}\beta^{1.97}\phi^{-2.03}$; where α = high severity burn + moderate severity burn as a fraction of total watershed (square miles/square miles); ψ = total drainage area (square miles); β = modified channel relief ratio (feet/feet); and ϕ = average basin elevation above mean sea level (thousands of feet). Note: α times ψ in above equation = hyper-effective drainage area. The points circled were 10-year events in the database (see Figure 1). The other 9 points were calculated using the other 9 sites in the database and the t-year equation with a storm return interval of 10 years.

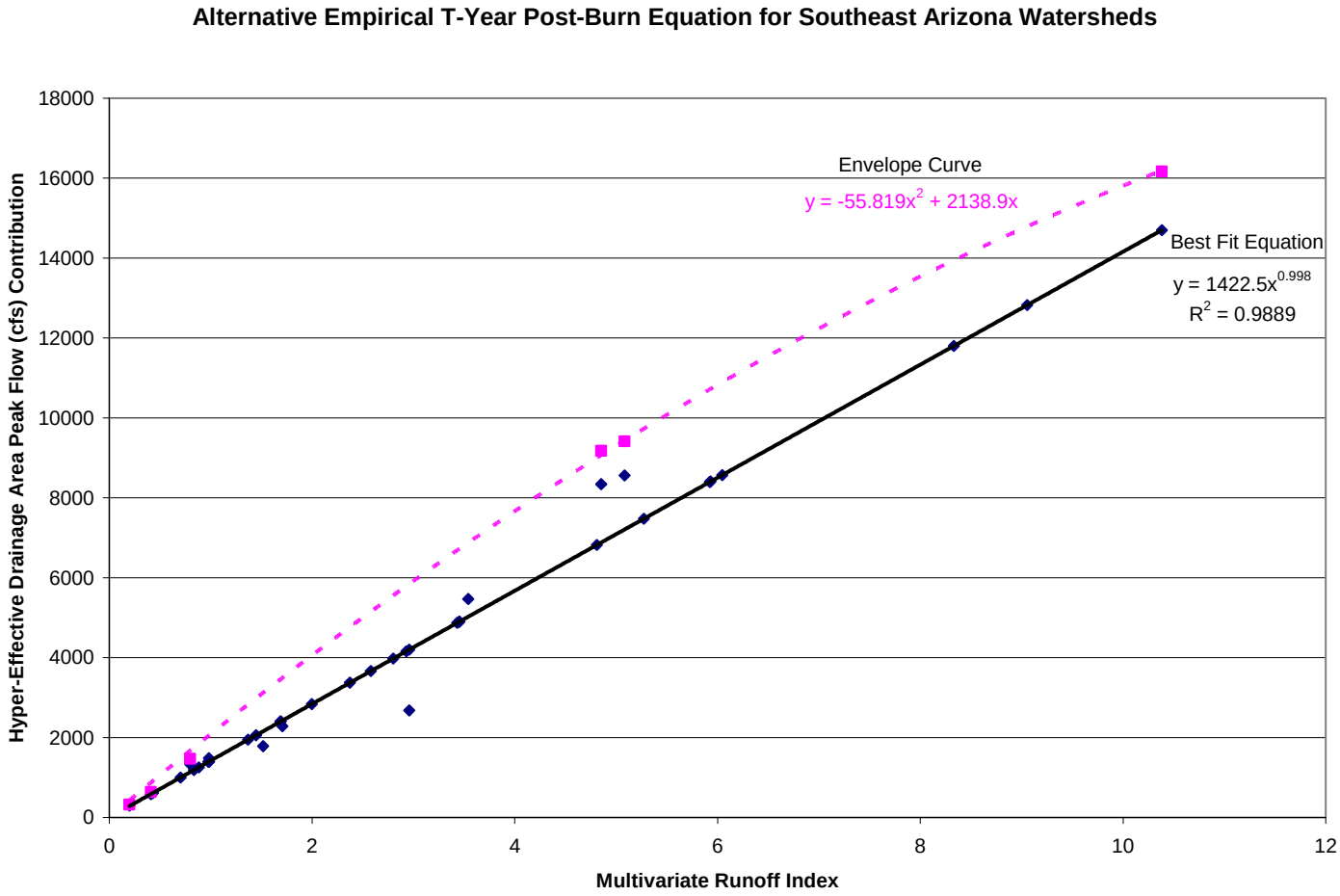

Figure 8: An empirical formula for when you know the forecast return interval of the rainfall developed using the four previous datasets combined (37 data points). The best-fit equation is essentially a straight line with a y-intercept of zero. Multivariate runoff index $=1000(\alpha\psi)^{0.51}\beta^{1.91}\phi^{-1.99}\lambda^{0.78}$; where α = high severity burn + moderate severity burn as a fraction of total watershed (square miles/square miles); ψ = total drainage area (square miles); β = modified channel relief ratio (feet/feet); ϕ = average basin elevation above mean sea level (thousands of feet) and λ = recurrence interval of rainfall (t-years). Note: α times ψ in above equation = hyper-effective drainage area.

Non Hyper-Effective Drainage Area Contribution (% of post-burn peak flow)						
BASIN	RANGE	Post-Burn Peak Flow (cfs)	Pre-Burn Peak Flow (cfs)	Hyper-Effective Drainage Area as a % of Total Drainage Area	Non Hyper-Effective Drainage Area as a % of Total Drainage Area	Non Hyper-Effective Drainage Area's Contribution as a % of Total Peak Flow
Noon Creek	Pinaleno Mountains	2684	19	77%	23%	0.2%
Wet Canyon	Pinaleno Mountains	1490	7.2	44%	56%	0.3%
Frye Creek	Pinaleno Mountains	1400	18.5	61%	39%	0.5%
Deadman Canyon	Pinaleno Mountains	5500	67.2	51%	49%	0.6%
Marijilda Canyon	Pinaleno Mountains	8470	313	59%	41%	1.5%
Cañada del Oro	Santa Catalina Mountains	1450	230	75%	25%	4%
Upper Campo Bonito	Santa Catalina Mountains	1900	586	80%	20%	6.2%
Romero Canyon	Santa Catalina Mountains	9500	1420	34%	66%	9.9%
Madera Canyon	Santa Rita Mountains	1526	224	15%	85%	12.5%
Sabino Creek near Mount Lemmon	Santa Catalina Mountains	350	119	55%	45%	15.3%
Alder Canyon at Ventana Windmill	Santa Catalina Mountains	3103	1260	35%	65%	26.4%

Figure 9: Percent of total post-burn peak flow contributed by non hyper-effective drainage area.

Pre-Burn and Post-Burn 2-Year, 5-Year, and 10-Year Peak Flows Best Fit Equation 3							
Watershed	Location	Pre-burn 2-year peak discharge (cfs)	Post-burn 2-year discharge (cfs)	Pre-burn 5-year peak discharge (cfs)	Post-burn 5-year discharge (cfs)	Pre-burn 10-year peak discharge (cfs)	Post-burn 10-year discharge (cfs)
Frye Creek	Pinaleno Mountains	26	2417	116	4922	254	8420
Deadman Canyon	Pinaleno Mountains	31	3694	137	7522	300	12867
Marijilda Canyon	Pinaleno Mountains	70	3419	313	7009 (8470)	686	12004
Noon Creek	Pinaleno Mountains	19	4204 (2685)	86	8569	188	14629
Wet Canyon	Pinaleno Mountains	10.2	2409	45.5	4896	100	8366
Upper Campo Bonito	Santa Catalina Mountains	156	651	376	1331	585	2274 (1872)
Sabino Creek near Mount Lemmon	Santa Catalina Mountains	119	340 (350)	278	702	431	1178
Alder Canyon at Ventana Windmill	Santa Catalina Mountains	523	1535	1260	3245 (3103)	1990	5426
Madera Canyon	Santa Rita Mountains	271	2185	657	4520	1030	7635
Romero Canyon	Santa Catalina Mountains	372	2322	902	4803	1420	7285 (9515)
Cañada del Oro	Santa Catalina Mountains	230	1450 (1450)	530	2964	810	5033

Figure 10: Total Watershed Pre-Burn and Post-Burn Peak Flows for 2-Year, 5-Year, and 10-Year Return Intervals. Reported values are shown in (blue). Other values were determined by using best fit Equation 3 to calculate peak from hyper-effective drainage area and then adding the peak from the remaining watershed (calculated by multiplying pre-burn peak by remaining area's percent of total watershed). The use of the best fit curve can result in values equal to or less than observed (e.g., 5-Year Peak Flow for Marijilda Canyon).

Pre-Burn and Post-Burn 2-Year, 5-Year, and 10-Year Peak Flows Envelope Curve Equation 12							
Watershed	Location	Pre-burn 2-year peak discharge (cfs)	Post-burn 2-year discharge (cfs)	Pre-burn 5-year peak discharge (cfs)	Post-burn 5-year discharge (cfs)	Pre-burn 10-year peak discharge (cfs)	Post-burn 10-year discharge (cfs)
Frye Creek	Pinaleno Mountains	26	3467	116	6769	254	10824
Deadman Canyon	Pinaleno Mountains	31	5163	137	9795	300	14940
Marijilda Canyon	Pinaleno Mountains	70	4793	313	9193 (8470)	686	14229
Noon Creek	Pinaleno Mountains	19	5844 (2685)	86	10913	188	16235
Wet Canyon	Pinaleno Mountains	10.2	3458	45.5	9262	100	10768
Upper Campo Bonito	Santa Catalina Mountains	156	945	376	1921	585	3234 (1872)
Sabino Creek near Mount Lemmon	Santa Catalina Mountains	119	480 (350)	278	992	431	1671
Alder Canyon at Ventana Windmill	Santa Catalina Mountains	523	2088	1260	4308 (3103)	1990	7084
Madera Canyon	Santa Rita Mountains	271	3056	657	6110	1030	9871
Romero Canyon	Santa Catalina Mountains	372	3227	902	6437	1420	10366 (9515)
Cañada del Oro	Santa Catalina Mountains	230	2096 (1450)	530	4186	810	6889

Figure 11: Total Watershed Pre-Burn and Post-Burn Peak Flows for 2-Year, 5-Year, and 10-Year Return Intervals. Reported values are shown in (blue). Other values were determined by using envelope curve Equation 12 to calculate peak from hyper-effective drainage area and then adding the peak from the remaining watershed (calculated by multiplying pre-burn peak by remaining area's percent of total watershed). The use of the envelope curve will result in estimates greater than the observed values.

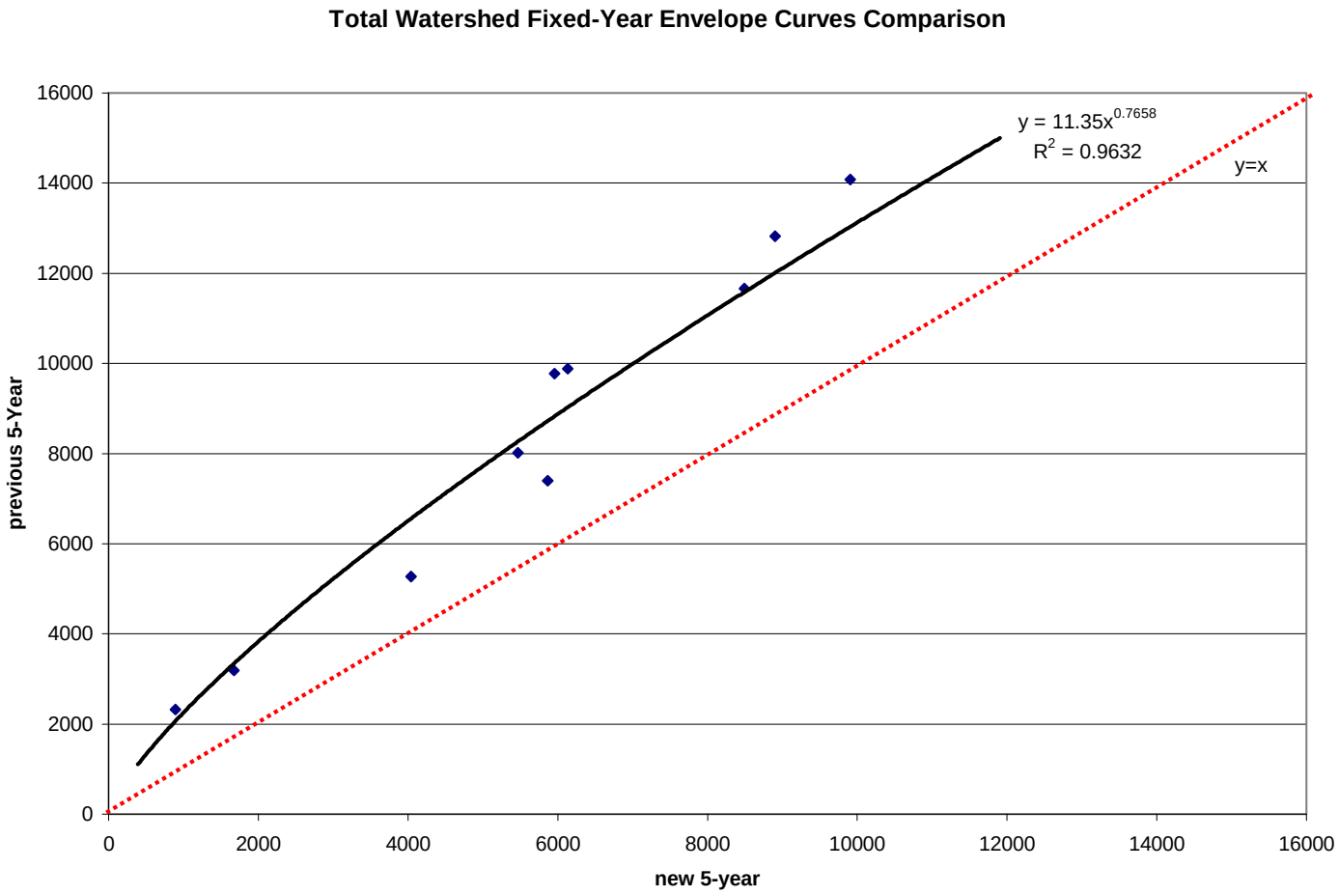

Figure 12: Comparisons of Fixed-Year Envelope Curves for 5-Year Post-Burn Events. New envelope curve is always less than previous envelope curve.

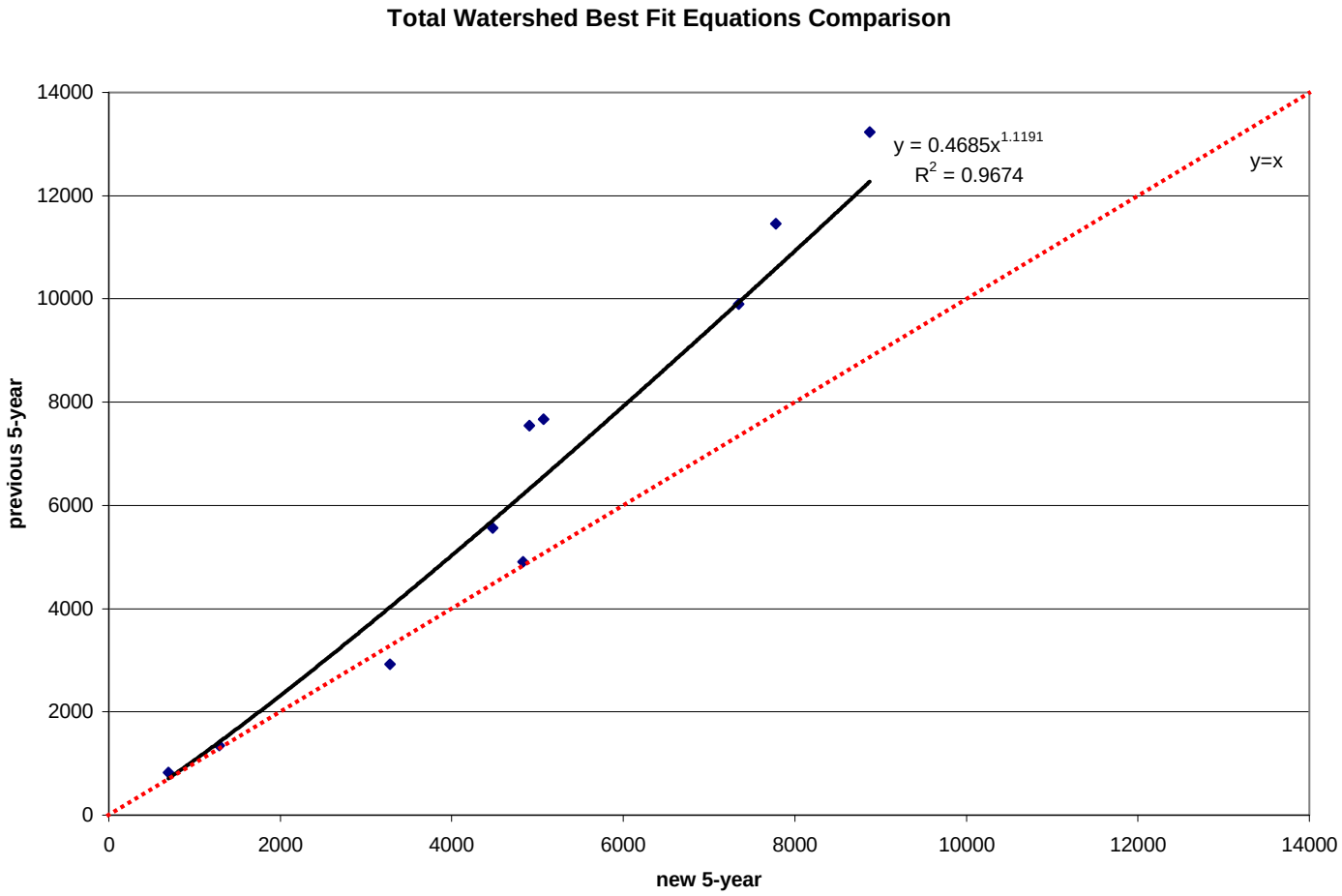

Figure 13: Comparison of Best Fit Equations for the 5-Year Post-Burn Events. Curves are essentially the same for four data points (Alder, Campo Bonito, Romero, and Sabino Canyons). New best-fit curve is less than previous best fit curve for the other 6 data points.

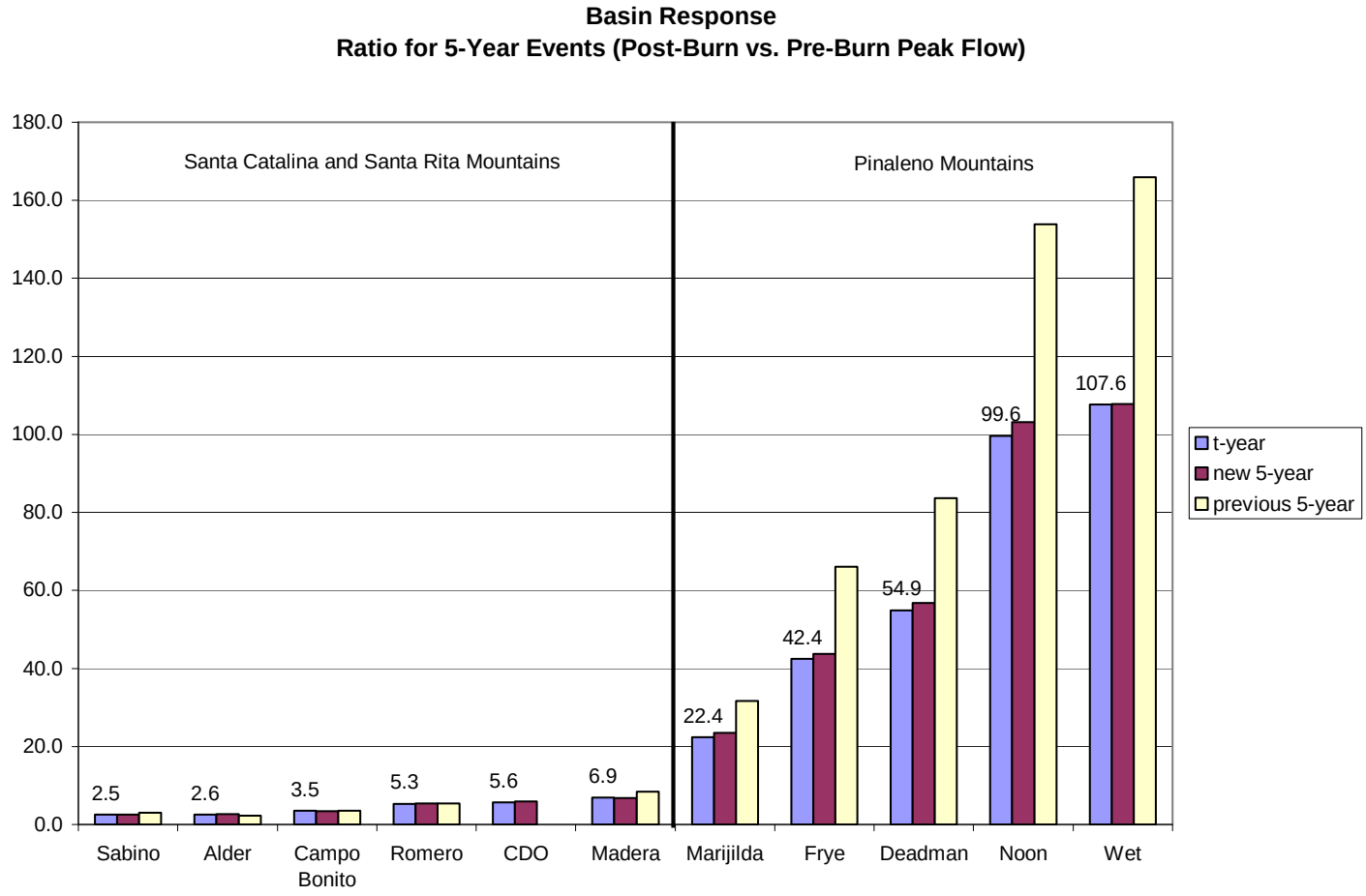

Figure 14: The 5-Year total watershed peak flow basin response under burn conditions for various watersheds in the Santa Catalina (Sabino, Alder, Campo Bonito, Romero, and Cañada del Oro), Santa Rita (Madera), and Pinaleno Mountains (Marijilda, Frye, Deadman, Noon, and Wet). Numerical values are shown for t-year equation. Post-Burn Response is up to 107.6 times greater than Pre-Burn Peak Flow.

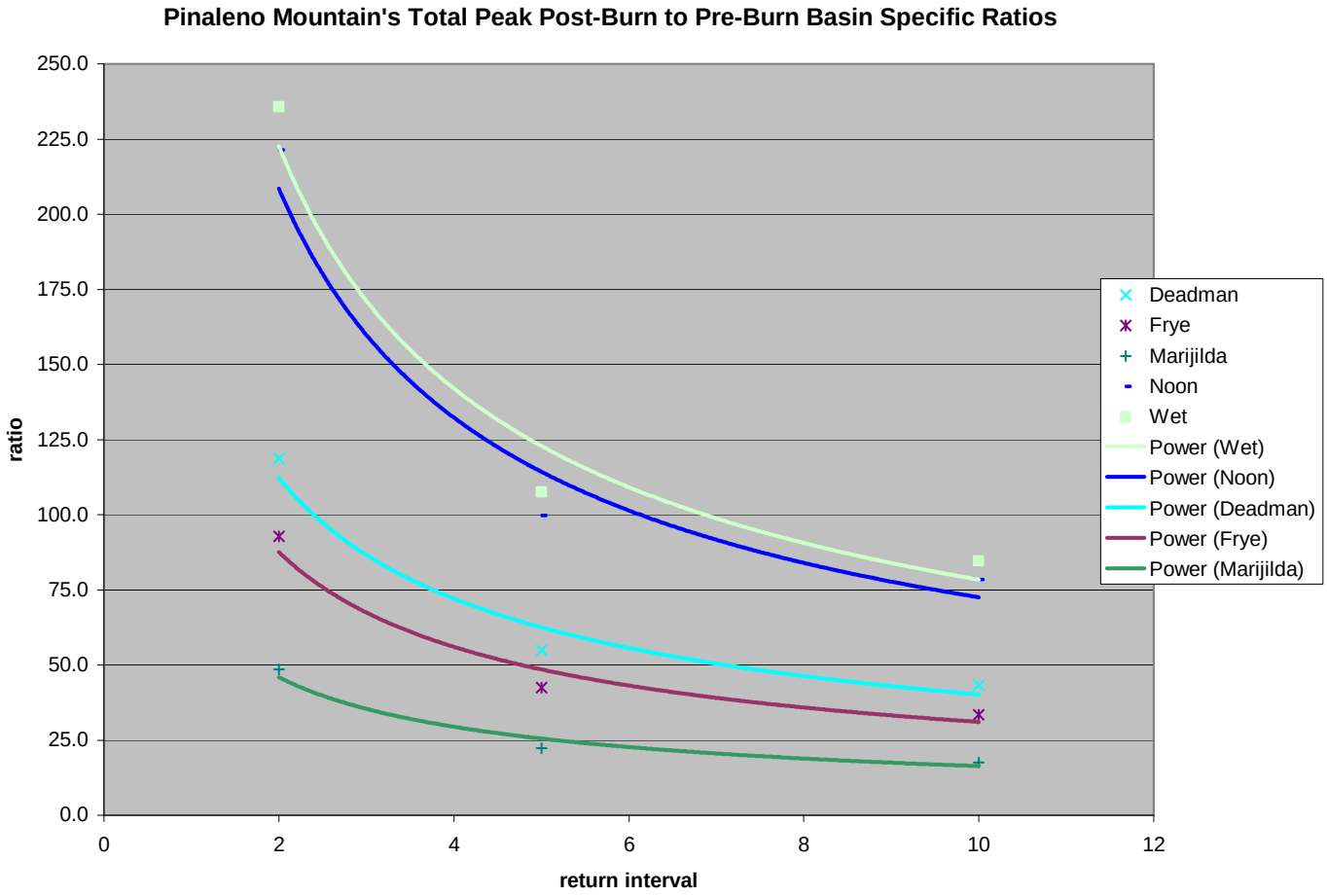

Figure 15: The Pinaleno Mountain basin specific total watershed post-burn to pre-burn peak flow ratios for return intervals 2, 5, and 10 years. All ratios are above 10. These ratios were calculated using the t-year best fit equation. The ratios decrease as return interval increases.

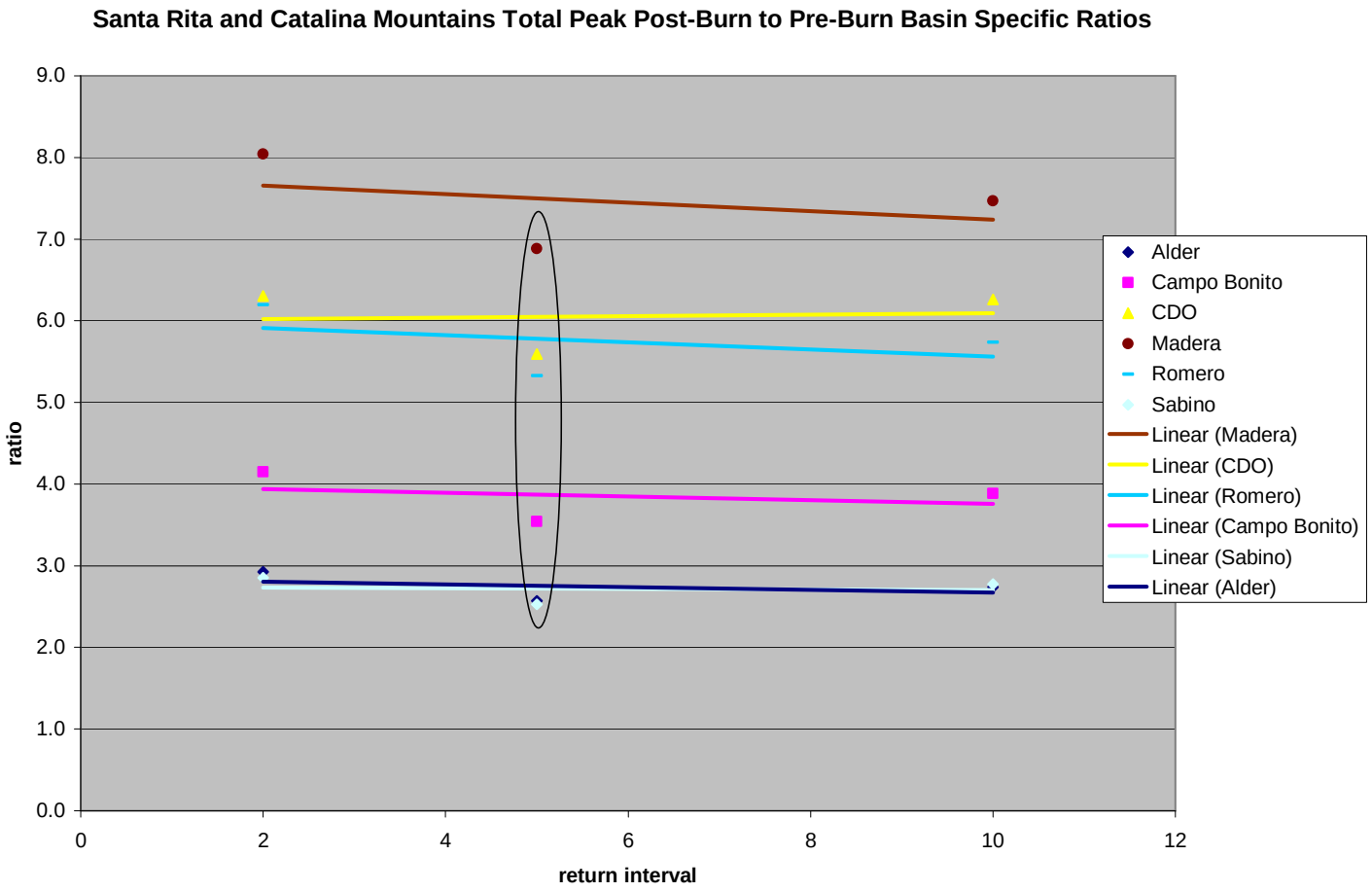

Figure 16: The Santa Rita and Catalina Mountains basin specific total watershed post-burn to pre-burn peak flow ratios for return intervals 2, 5, and 10 years. All ratios are below 10. These ratios were calculated using the t-year best fit equation. The values decrease as the return interval increases. The circled 5-year ratios are assumed to be too low. This indicates that perhaps the flood peak flow values for Alder and Marijilda Canyons calculated using indirect methods were too low. CDO = Cañada del Oro.

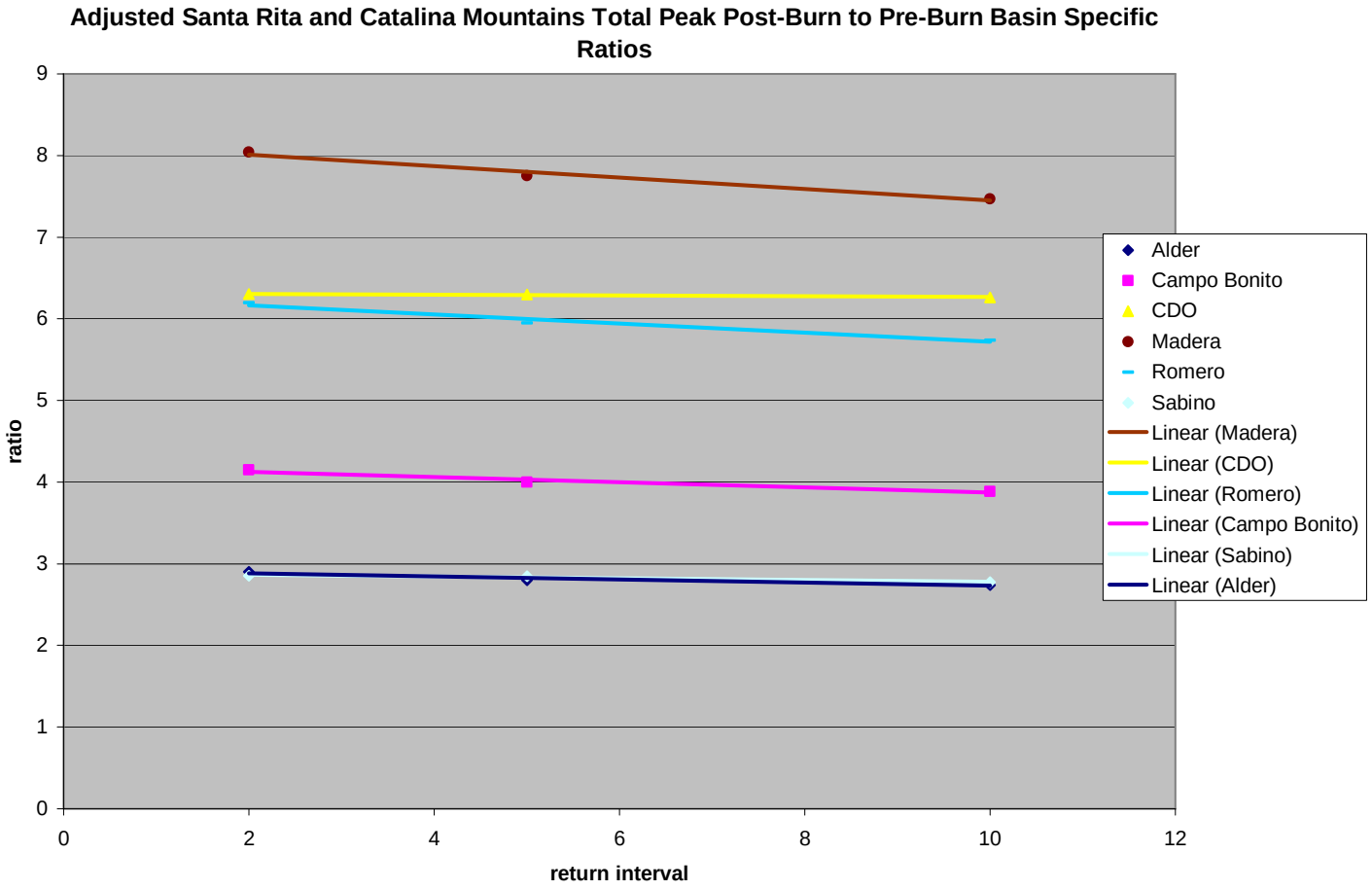

Figure 17: The Santa Rita and Catalina Mountains basin specific total watershed post-burn to pre-burn peak flow ratios for return intervals 2, 5, and 10 years. All ratios are below 10. These adjusted ratios were calculated using the t-year best fit equation and slightly increasing the results of the 5-year values (the values were increased 10% to 15.5%. Such an increase is within the reported error of 25%. In general, the values decrease as the return interval increases. The results are presented here for comparison with Figure 15. CDO = Cañada del Oro.

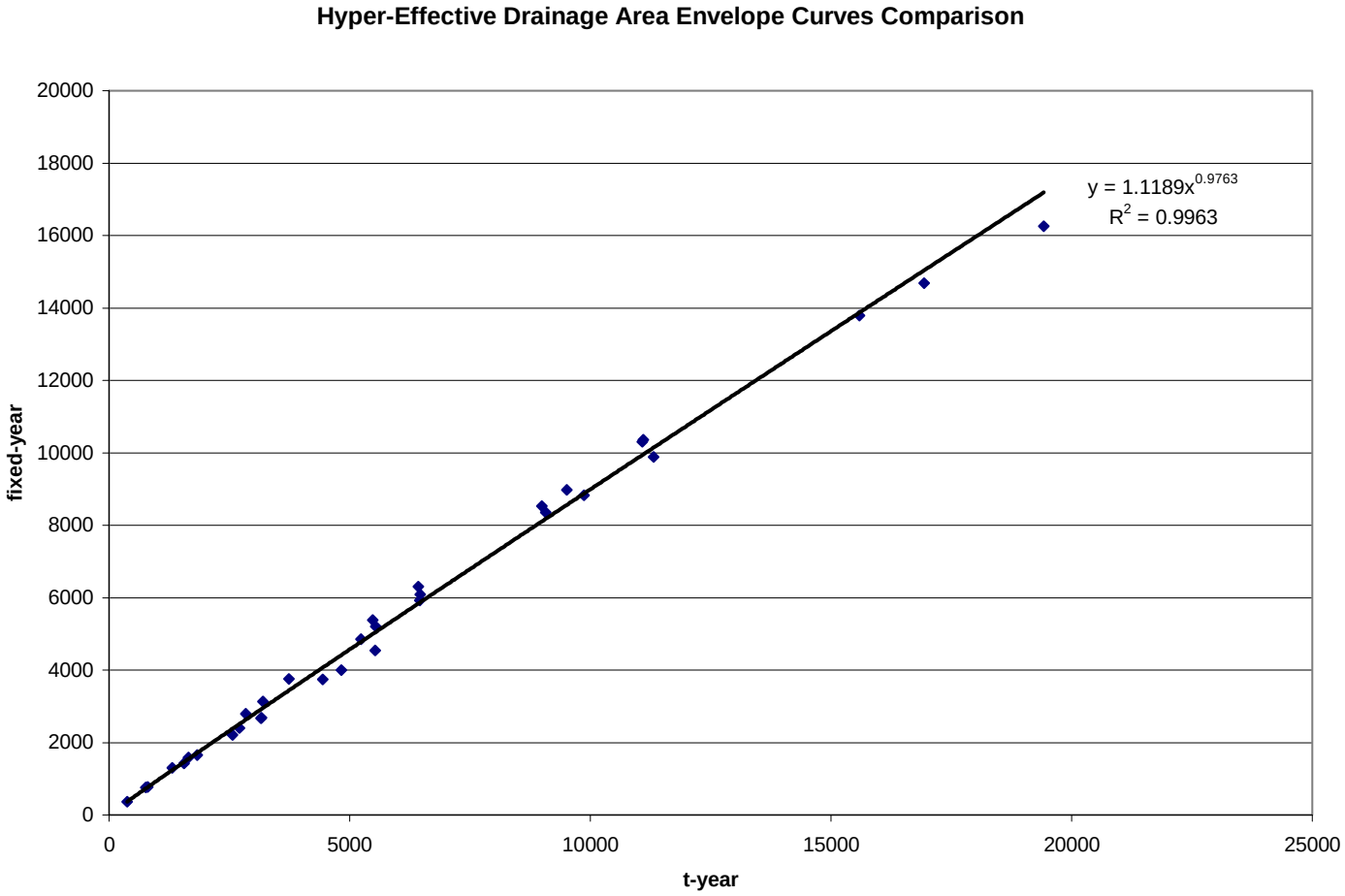

Figure 18: Comparison of Envelope Equations for Hyper-Effective Drainage Area Peak Flow (cfs) Contribution. The fixed-year equations (Equations 4, 6, and 10) result in values slightly greater than the corresponding t-year equation (Equation 2) values.

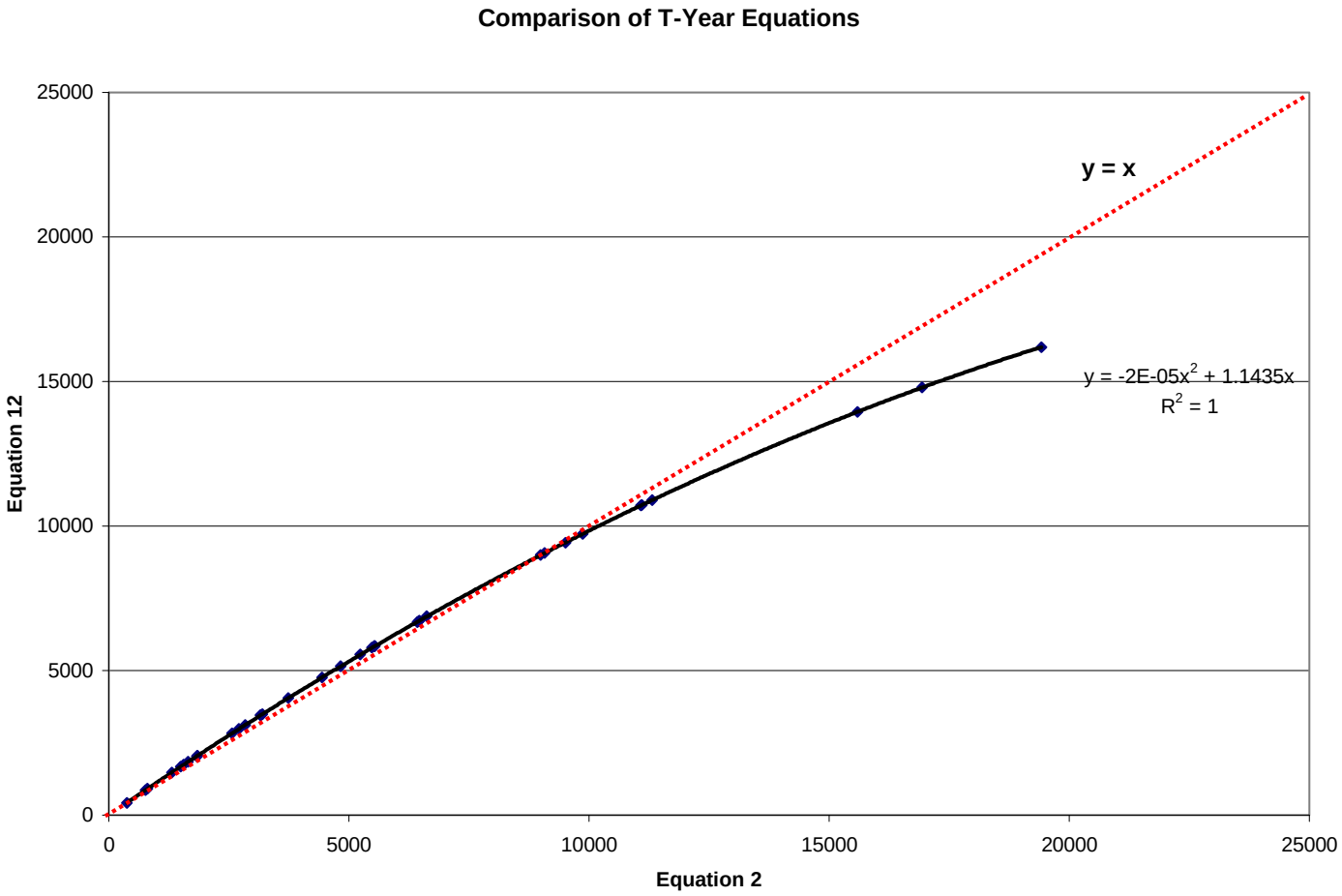

Figure 19: Comparison the Two T-Year Envelope Equations for Hyper-Effective Drainage Area Peak Flow (cfs) Contribution. The two curves provide essentially the same results for the basins with hyper-effective drainage area peak flows less than 11500 cfs. For the basin with peak flows greater than 11500 cfs, Envelope Curve 12 provides the lower values.

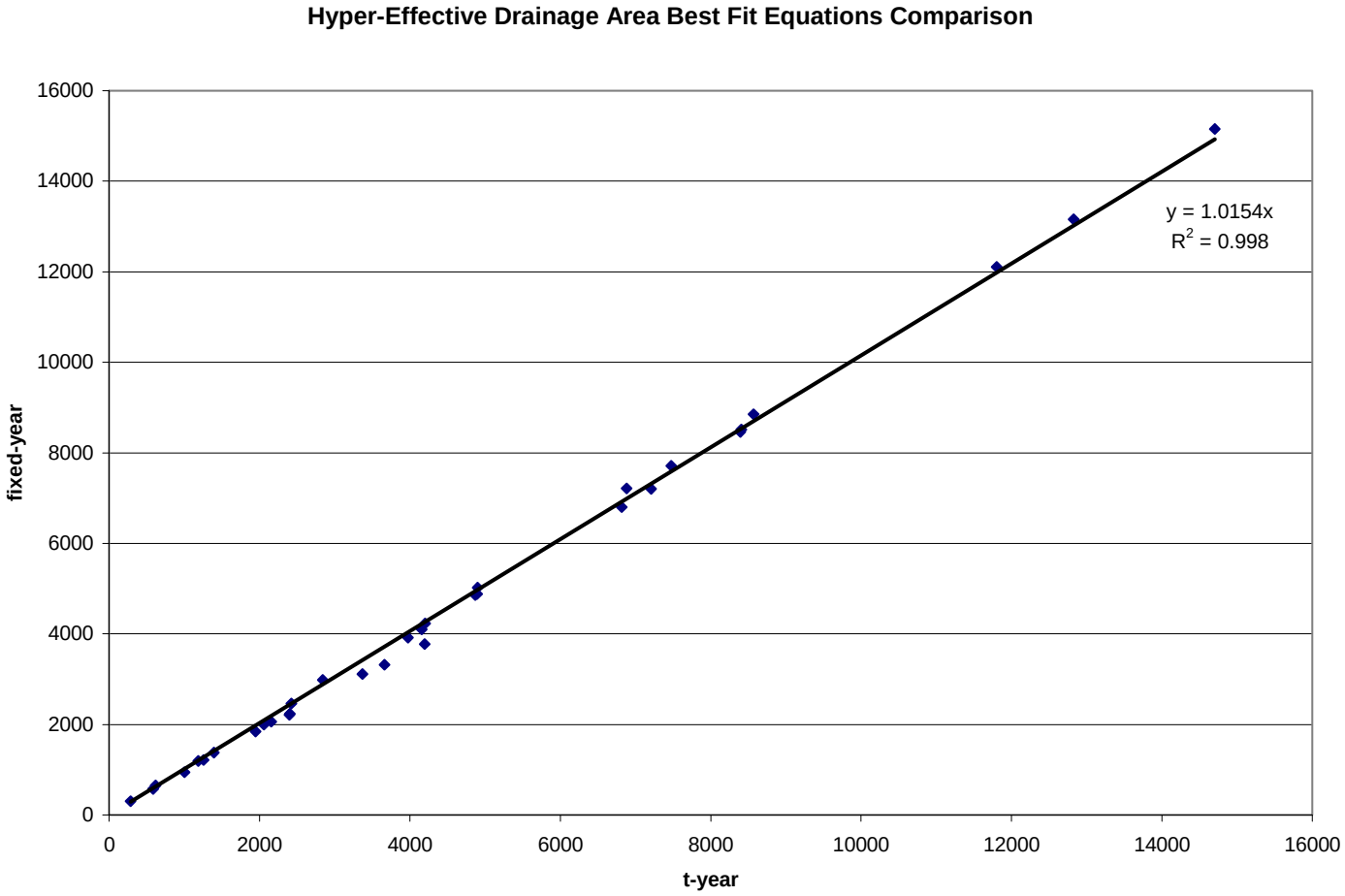

Figure 20: Comparison of Best Fit Equations for Hyper-Effective Drainage Area Peak Flow (cfs) Contribution. The fixed-year equations (Equations 5, 7, and 11) and the t-year equation (Equation 3) result in essentially the same values.

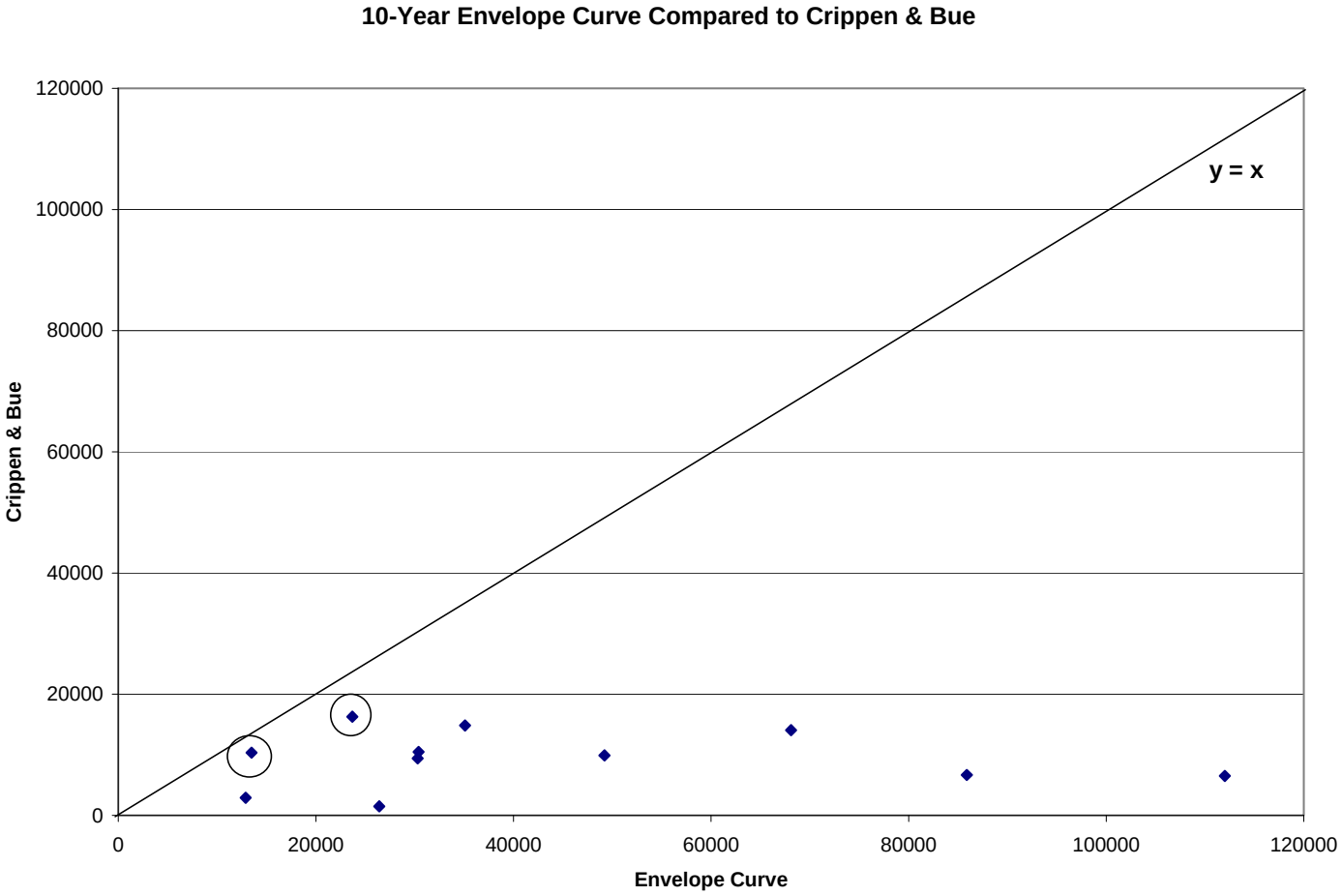

Figure 21: Comparison of the results of Envelope Curve for the 10-year return interval and adding the peak for the remaining watershed with the results for maximum flood flow calculated using the method presented in Crippen and Bue (1977). All Envelope Curve values are below the corresponding maximum flood flows. However, the 10-year values for Noon and Wet Canyons (circled on the figure) approach maximum flood flow.

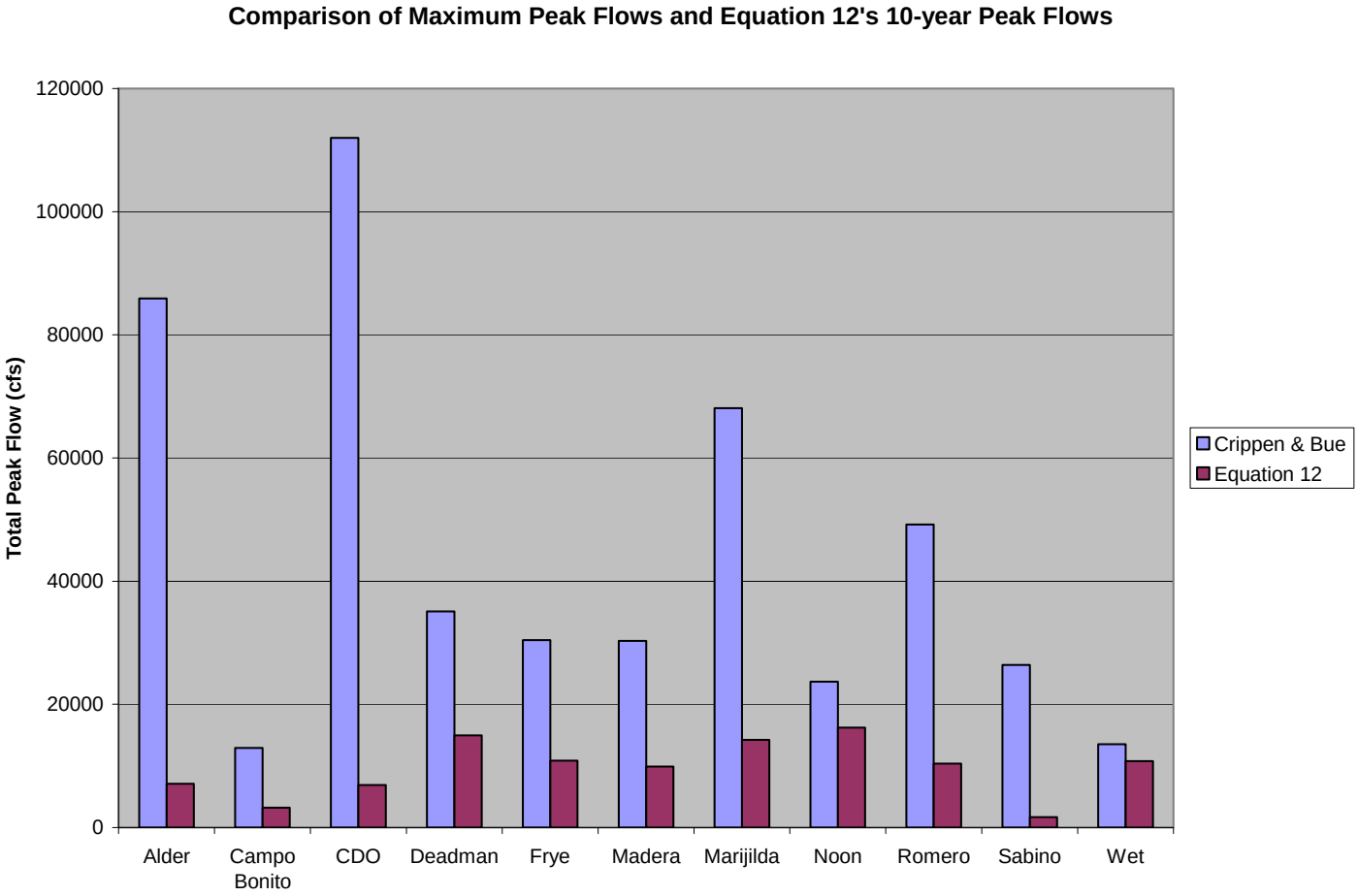

Figure 22: Comparison of the results of Alternative T-Year Envelope Curve (Equation 12) using a return interval of 10 years and adding the peak for the remaining watershed with the results for maximum flood flow calculated using the method presented in Crippen and Bue (1977). All Envelope Curve values are below the corresponding maximum flood flows. However, the 10-year values for Noon and Wet Canyons approach maximum flood flow. CDO = Cañada del Oro.

APPENDIX III – STEPS FOR ADAPTING METHOLOGY

Step 1: Collect data for new area similar to data presented in Figures 1 and 2 (suggest at least 10 events).

Step 2: Select variables. Suggest the four used here: *hyper-effective drainage area, average basin elevation, modified channel relief ratio, and return interval of the forecast rainfall event*, or similar variables. With regard to the modified channel relief ratio:

1) for low elevation coastal ranges it might be useful to use the average slope of the basin along the first order channel measured from the ridge to the basin outlet and
2) for high elevation interior ranges it may be useful to use the average slope of the basin along the first order channel measured from 1,250 feet (or some uniformed distance) below tree line to the basin outlet.

Step 3: Enter data into spreadsheet.

Step 4: Use regression data analysis tool to determine coefficients for the selected variables.

Step 5: Calculate the multivariate runoff index in the spreadsheet.

Step 6: Plot a figure like Figure 3.

Step 7: Develop an envelope curve by selecting a subset of the data points and then fitting a curve through 1.1 times the values for the selected points. This process should be repeated several times until a useful equation is created.

NOAA TECHNICAL MEMORANDA National Weather Service, Western Region Subseries

The National Weather Service (NWS) Western Region (WR) Subseries provides an informal medium for the documentation and quick dissemination of results not appropriate, or not yet ready, for formal publication. The series is used to report on work in progress, to describe technical procedures and practices, or to relate progress to a limited audience. These Technical Memoranda will report on investigations devoted primarily to regional and local problems of interest mainly to personnel, and hence will not be widely distributed.

Papers 1 to 25 are in the former series, ESSA Technical Memoranda, Western Region Technical Memoranda (WRTM); papers 24 to 59 are in the former series, ESSA Technical Memoranda, Weather Bureau Technical Memoranda (WBTM). Beginning with 60, the papers are part of the series, NOAA Technical Memoranda NWS. Out-of-print memoranda are not listed.

Papers 2 to 22, except for 5 (revised edition), are available from the National Weather Service Western Region, Scientific Services Division, 125 South State Street - Rm 1311, Salt Lake City, Utah 84138-1102. Paper 5 (revised edition), and all others beginning with 25 are available from the National Technical Information Service, U.S. Department of Commerce, Sills Building, 5285 Port Royal Road, Springfield, Virginia 22161. Prices vary for all paper copies; microfiche are $3.50. Order by accession number shown in parentheses at end of each entry.

ESSA Technical Memoranda (WRTM)

2 Climatological Precipitation Probabilities. Compiled by Lucianne Miller, December 1965.
3 Western Region Pre- and Post-FP-3 Program, December 1, 1965, to February 20, 1966. Edward D. Diemer, March 1966.
5 Station Descriptions of Local Effects on Synoptic Weather Patterns. Philip Williams, Jr., April 1966 (Revised November 1967, October 1969). (PB-17800)
8 Interpreting the RAREP. Herbert P. Benner, May 1966 (Revised January 1967).
11 Some Electrical Processes in the Atmosphere. J. Latham, June 1966.
17 A Digitalized Summary of Radar Echoes within 100 Miles of Sacramento, California. J. A. Youngberg and L. B. Overaas, December 1966.
21 An Objective Aid for Forecasting the End of East Winds in the Columbia Gorge, July through October. D. John Coparanis, April 1967.
22 Derivation of Radar Horizons in Mountainous Terrain. Roger G. Pappas, April 1967.

ESSA Technical Memoranda, Weather Bureau Technical Memoranda (WBTM)

25 Verification of Operation Probability of Precipitation Forecasts, April 1966-March 1967. W. W. Dickey, October 1967. (PB-176240)
26 A Study of Winds in the Lake Mead Recreation Area. R. P. Augulis, January 1968. (PB-177830)
28 Weather Extremes. R. J. Schmidli, April 1968 (Revised March 1986). (PB86 177672/AS). (Revised October 1991 - PB92-115062/AS)
29 Small-Scale Analysis and Prediction. Philip Williams, Jr., May 1968. (PB178425)
30 Numerical Weather Prediction and Synoptic Meteorology. CPT Thomas D. Murphy, USAF, May 1968. (AD 673365)
31 Precipitation Detection Probabilities by Salt Lake ARTC Radars. Robert K. Belesky, July 1968. (PB 179084)
32 Probability Forecasting--A Problem Analysis with Reference to the Portland Fire Weather District. Harold S. Ayer, July 1968. (PB 179289)
36 Temperature Trends in Sacramento--Another Heat Island. Anthony D. Lentini, February 1969. (PB 183055)
37 Disposal of Logging Residues Without Damage to Air Quality. Owen P. Cramer, March 1969. (PB 183057)
39 Upper-Air Lows Over Northwestern United States. A.L. Jacobson, April 1969. PB 184296)
40 The Man-Machine Mix in Applied Weather Forecasting in the 1970s. L.W. Snellman, August 1969. (PB 185068)
43 Forecasting Maximum Temperatures at Helena, Montana. David E. Olsen, October 1969. (PB 185762)
44 Estimated Return Periods for Short-Duration Precipitation in Arizona. Paul C. Kangieser, October 1969. (PB 187763)
46 Applications of the Net Radiometer to Short-Range Fog and Stratus Forecasting at Eugene, Oregon. L. Yee and E. Bates, December 1969. (PB 190476)
47 Statistical Analysis as a Flood Routing Tool. Robert J.C. Burnash, December 1969. (PB 188744)
48 Tsunami. Richard P. Augulis, February 1970. (PB 190157)
49 Predicting Precipitation Type. Robert J.C. Burnash and Floyd E. Hug, March 1970. (PB 190962)
50 Statistical Report on Aeroallergens (Pollens and Molds) Fort Huachuca, Arizona, 1969. Wayne S. Johnson, April 1970. (PB 191743)
51 Western Region Sea State and Surf Forecaster's Manual. Gordon C. Shields and Gerald B. Burdwell, July 1970. (PB 193102)
52 Sacramento Weather Radar Climatology. R.G. Pappas and C. M. Veliquette, July 1970. (PB 193347)
54 A Refinement of the Vorticity Field to Delineate Areas of Significant Precipitation. Barry B. Aronovitch, August 1970.
55 Application of the SSARR Model to a Basin without Discharge Record. Vail Schermerhorn and Donal W. Kuehl, August 1970. (PB 194394)
56 Areal Coverage of Precipitation in Northwestern Utah. Philip Williams, Jr., and Werner J. Heck, September 1970. (PB 194389)
57 Preliminary Report on Agricultural Field Burning vs. Atmospheric Visibility in the Willamette Valley of Oregon. Earl M. Bates and David O. Chilcote, September 1970. (PB 194710)
58 Air Pollution by Jet Aircraft at Seattle-Tacoma Airport. Wallace R. Donaldson, October 1970. (COM 71 00017)
59 Application of PE Model Forecast Parameters to Local-Area Forecasting. Leonard W. Snellman, October 1970. (COM 71 00016)
60 An Aid for Forecasting the Minimum Temperature at Medford, Oregon, Arthur W. Fritz, October 1970. (COM 71 00120)
63 700-mb Warm Air Advection as a Forecasting Tool for Montana and Northern Idaho. Norris E. Woerner, February 1971. (COM 71 00349)
64 Wind and Weather Regimes at Great Falls, Montana. Warren B. Price, March 1971.
65 Climate of Sacramento, California. Laura Masters-Bevan. NWSO Sacramento, November 1998 (6th Revision. (PB99-118424)
66 A Preliminary Report on Correlation of ARTCC Radar Echoes and Precipitation. Wilbur K. Hall, June 1971. (COM 71 00829)
69 National Weather Service Support to Soaring Activities. Ellis Burton, August 1971. (COM 71 00956)
71 Western Region Synoptic Analysis-Problems and Methods. Philip Williams, Jr., February 1972. (COM 72 10433)
74 Thunderstorms and Hail Days Probabilities in Nevada. Clarence M. Sakamoto, April 1972. (COM 72 10554)
75 A Study of the Low Level Jet Stream of the San Joaquin Valley. Ronald A. Willis and Philip Williams, Jr., May 1972. (COM 72 10707)
76 Monthly Climatological Charts of the Behavior of Fog and Low Stratus at Los Angeles International Airport. Donald M. Gales, July 1972. (COM 72 11140)
77 A Study of Radar Echo Distribution in Arizona During July and August. John E. Hales, Jr., July 1972. (COM 72 11136)
78 Forecasting Precipitation at Bakersfield, California, Using Pressure Gradient Vectors. Earl T. Riddiough, July 1972. (COM 72 11146)
79 Climate of Stockton, California. Robert C. Nelson, July 1972. (COM 72 10920)
80 Estimation of Number of Days Above or Below Selected Temperatures. Clarence M. Sakamoto, October 1972. (COM 72 10021)
81 An Aid for Forecasting Summer Maximum Temperatures at Seattle, Washington. Edgar G. Johnson, November 1972. (COM 73 10150)
82 Flash Flood Forecasting and Warning Program in the Western Region. Philip Williams, Jr., Chester L. Glenn, and Roland L. Raetz, December 1972, (Revised March 1978). (COM 73 10251)
83 A comparison of Manual and Semiautomatic Methods of Digitizing Analog Wind Records. Glenn E. Rasch, March 1973. (COM 73 10669)
86 Conditional Probabilities for Sequences of Wet Days at Phoenix, Arizona. Paul C. Kangieser, June 1973. (COM 73 11264)
87 A Refinement of the Use of K-Values in Forecasting Thunderstorms in Washington and Oregon. Robert Y.G. Lee, June 1973. (COM 73 11276)
89 Objective Forecast Precipitation Over the Western Region of the United States. Julia N. Paegle and Larry P. Kierulff, September 1973. (COM 73 11946/3AS)
91 Arizona "Eddy" Tornadoes. Robert S. Ingram, October 1973. (COM 73 10465)
92 Smoke Management in the Willamette Valley. Earl M. Bates, May 1974. (COM 74 11277/AS)
93 An Operational Evaluation of 500-mb Type Regression Equations. Alexander E. MacDonald, June 1974. (COM 74 11407/AS)
94 Conditional Probability of Visibility Less than One-Half Mile in Radiation Fog at Fresno, California. John D. Thomas, August 1974. (COM 74 11555/AS)
95 Climate of Flagstaff, Arizona. Paul W. Sorenson, and updated by Reginald W. Preston, January 1987. (PB87 143160/AS) (Revised August 2002 3rd Revision)
96 Map type Precipitation Probabilities for the Western Region. Glenn E. Rasch and Alexander E. MacDonald, February 1975. (COM 75 10428/AS)
97 Eastern Pacific Cut-Off Low of April 21-28, 1974. William J. Alder and George R. Miller, January 1976. (PB 250 711/AS)
98 Study on a Significant Precipitation Episode in Western United States. Ira S. Brenner, April 1976. (COM 75 10719/AS)
99 A Study of Flash Flood Susceptibility-A Basin in Southern Arizona. Gerald Williams, August 1975. (COM 75 11360/AS)
102 A Set of Rules for Forecasting Temperatures in Napa and Sonoma Counties. Wesley L. Tuft, October 1975. (PB 246 902/AS)

103 Application of the National Weather Service Flash-Flood Program in the Western Region. Gerald Williams, January 1976. (PB 253 053/AS)
104 Objective Aids for Forecasting Minimum Temperatures at Reno, Nevada, During the Summer Months. Christopher D. Hill, January 1976. (PB 252 866/AS)
105 Forecasting the Mono Wind. Charles P. Ruscha, Jr., February 1976. (PB 254 650)
106 Use of MOS Forecast Parameters in Temperature Forecasting. John C. Plankinton, Jr., March 1976. (PB 254 649)
107 Map Types as Aids in Using MOS PoPs in Western United States. Ira S. Brenner, August 1976. (PB 259 594)
108 Other Kinds of Wind Shear. Christopher D. Hill, August 1976. (PB 260 437/AS)
109 Forecasting North Winds in the Upper Sacramento Valley and Adjoining Forests. Christopher E. Fontana, September 1976. (PB 273 677/AS)
110 Cool Inflow as a Weakening Influence on Eastern Pacific Tropical Cyclones. William J. Denney, November 1976. (PB 264 655/AS)
112 The MAN/MOS Program. Alexander E. MacDonald, February 1977. (PB 265 941/AS)
113 Winter Season Minimum Temperature Formula for Bakersfield, California, Using Multiple Regression. Michael J. Oard, February 1977. (PB 273 694/AS)
114 Tropical Cyclone Kathleen. James R. Fors, February 1977. (PB 273 676/AS)
116 A Study of Wind Gusts on Lake Mead. Bradley Colman, April 1977. (PB 268 847)
117 The Relative Frequency of Cumulonimbus Clouds at the Nevada Test Site as a Function of K-Value. R.F. Quiring, April 1977. (PB 272 831)
118 Moisture Distribution Modification by Upward Vertical Motion. Ira S. Brenner, April 1977. (PB 268 740)
119 Relative Frequency of Occurrence of Warm Season Echo Activity as a Function of Stability Indices Computed from the Yucca Flat, Nevada, Rawinsonde. Darryl Randerson, June 1977. (PB 271 290/AS)
121 Climatological Prediction of Cumulonimbus Clouds in the Vicinity of the Yucca Flat Weather Station. R.F. Quiring, June 1977. (PB 271 704/AS)
122 A Method for Transforming Temperature Distribution to Normality. Morris S. Webb, Jr., June 1977. (PB 271 742/AS)
124 Statistical Guidance for Prediction of Eastern North Pacific Tropical Cyclone Motion - Part I. Charles J. Neumann and Preston W. Leftwich, August 1977. (PB 272 661)
125 Statistical Guidance on the Prediction of Eastern North Pacific Tropical Cyclone Motion - Part II. Preston W. Leftwich and Charles J. Neumann, August 1977. (PB 273 155/AS)
126 Climate of San Francisco. E. Jan Null, February 1978. (Revised by George T. Pericht, April 1988 and January 1995). (PB88 208624/AS)
127 Development of a Probability Equation for Winter-Type Precipitation Patterns in Great Falls, Montana. Kenneth B. Mielke, February 1978. (PB 281 387/AS)
128 Hand Calculator Program to Compute Parcel Thermal Dynamics. Dan Gudgel, April 1978. (PB 283 080/AS)
129 Fire whirls. David W. Goens, May 1978. (PB 283 866/AS)
130 Flash-Flood Procedure. Ralph C. Hatch and Gerald Williams, May 1978. (PB 286 014/AS)
131 Automated Fire-Weather Forecasts. Mark A. Mollner and David E. Olsen, September 1978. (PB 289 916/AS)
132 Estimates of the Effects of Terrain Blocking on the Los Angeles WSR-74C Weather Radar. R.G. Pappas, R.Y. Lee, B.W. Finke, October 1978. (PB 289767/AS)
133 Spectral Techniques in Ocean Wave Forecasting. John A. Jannuzzi, October 1978. (PB291317/AS)
134 Solar Radiation. John A. Jannuzzi, November 1978. (PB291195/AS)
135 Application of a Spectrum Analyzer in Forecasting Ocean Swell in Southern California Coastal Waters. Lawrence P. Kierulff, January 1979. (PB292716/AS)
136 Basic Hydrologic Principles. Thomas L. Dietrich, January 1979. (PB292247/AS)
137 LFM 24-Hour Prediction of Eastern Pacific Cyclones Refined by Satellite Images. John R. Zimmerman and Charles P. Ruscha, Jr., January 1979. (PB294324/AS)
138 A Simple Analysis/Diagnosis System for Real Time Evaluation of Vertical Motion. Scott Heflick and James R. Fors, February 1979. (PB294216/AS)
139 Aids for Forecasting Minimum Temperature in the Wenatchee Frost District. Robert S. Robinson, April 1979. (PB298339/AS)
140 Influence of Cloudiness on Summertime Temperatures in the Eastern Washington Fire Weather district. James Holcomb, April 1979. (PB298674/AS)
141 Comparison of LFM and MFM Precipitation Guidance for Nevada During Doreen. Christopher Hill, April 1979. (PB298613/AS)
142 The Usefulness of Data from Mountaintop Fire Lookout Stations in Determining Atmospheric Stability. Jonathan W. Corey, April 1979. (PB298899/AS)
143 The Depth of the Marine Layer at San Diego as Related to Subsequent Cool Season Precipitation Episodes in Arizona. Ira S. Brenner, May 1979. (PB298817/AS)
144 Arizona Cool Season Climatological Surface Wind and Pressure Gradient Study. Ira S. Brenner, May 1979. (PB298900/AS)
146 The BART Experiment. Morris S. Webb, October 1979. (PB80 155112)
147 Occurrence and Distribution of Flash Floods in the Western Region. Thomas L. Dietrich, December 1979. (PB80 160344)
149 Misinterpretations of Precipitation Probability Forecasts. Allan H. Murphy, Sarah Lichtenstein, Baruch Fischhoff, and Robert L. Winkler, February 1980. (PB80 174576)
150 Annual Data and Verification Tabulation - Eastern and Central North Pacific Tropical Storms and Hurricanes 1979. Emil B. Gunther and Staff, EPHC, April 1980. (PB80 220486)
151 NMC Model Performance in the Northeast Pacific. James E. Overland, PMEL-ERL, April 1980. (PB80 196033)
152 Climate of Salt Lake City, Utah. William J. Alder, Sean T. Buchanan, William Cope (Retired), James A. Cisco, Craig C. Schmidt, Alexander R. Smith (Retired), Wilbur E. Figgins (Retired), February 1998 - Seventh Revision (PB98-130727)
153 An Automatic Lightning Detection System in Northern California. James E. Rea and Chris E. Fontana, June 1980. (PB80 225592)
154 Regression Equation for the Peak Wind Gust 6 to 12 Hours in Advance at Great Falls During Strong Downslope Wind Storms. Michael J. Oard, July 1980. (PB91 108367)
155 A Raininess Index for the Arizona Monsoon. John H. Ten Harkel, July 1980. (PB81 106494)
156 The Effects of Terrain Distribution on Summer Thunderstorm Activity at Reno, Nevada. Christopher Dean Hill, July 1980. (PB81 102501)
157 An Operational Evaluation of the Scofield/Oliver Technique for Estimating Precipitation Rates from Satellite Imagery. Richard Ochoa, August 1980. (PB81 108227)
158 Hydrology Practicum. Thomas Dietrich, September 1980. (PB81 134033)
159 Tropical Cyclone Effects on California. Arnold Court, October 1980. (PB81 133779)
160 Eastern North Pacific Tropical Cyclone Occurrences During Intraseasonal Periods. Preston W. Leftwich and Gail M. Brown, February 1981. (PB81 205494)
161 Solar Radiation as a Sole Source of Energy for Photovoltaics in Las Vegas, Nevada, for July and December. Darryl Randerson, April 1981. (PB81 224503)
162 A Systems Approach to Real-Time Runoff Analysis with a Deterministic Rainfall-Runoff Model. Robert J.C. Burnash and R. Larry Ferral, April 1981. (PB81 224495)
163 A Comparison of Two Methods for Forecasting Thunderstorms at Luke Air Force Base, Arizona. LTC Keith R. Cooley, April 1981. (PB81 225393)
164 An Objective Aid for Forecasting Afternoon Relative Humidity Along the Washington Cascade East Slopes. Robert S. Robinson, April 1981. (PB81 23078)
165 Annual Data and Verification Tabulation, Eastern North Pacific Tropical Storms and Hurricanes 1980. Emil B. Gunther and Staff, May 1981. (PB82 230336)
166 Preliminary Estimates of Wind Power Potential at the Nevada Test Site. Howard G. Booth, June 1981. (PB82 127036)
167 ARAP User's Guide. Mark Mathewson, July 1981, Revised September 1981. (PB82 196783)
168 Forecasting the Onset of Coastal Gales Off Washington-Oregon. John R. Zimmerman and William D. Burton, August 1981. (PB82 127051)
169 A Statistical-Dynamical Model for Prediction of Tropical Cyclone Motion in the Eastern North Pacific Ocean. Preston W. Leftwich, Jr., October 1981. (PB82195298)
170 An Enhanced Plotter for Surface Airways Observations. Andrew J. Spry and Jeffrey L. Anderson, October 1981. (PB82 153883)
171 Verification of 72-Hour 500-MB Map-Type Predictions. R.F. Quiring, November 1981. (PB82-158098)
172 Forecasting Heavy Snow at Wenatchee, Washington. James W. Holcomb, December 1981. (PB82-177783)
173 Central San Joaquin Valley Type Maps. Thomas R. Crossan, December 1981. (PB82 196064)
174 ARAP Test Results. Mark A. Mathewson, December 1981. (PB82 198103)
176 Approximations to the Peak Surface Wind Gusts from Desert Thunderstorms. Darryl Randerson, June 1982. (PB82 253089)
177 Climate of Phoenix, Arizona. Robert J. Schmidli and Austin Jamison, April 1969 (Revised July 1996). (PB96-191614)
178 Annual Data and Verification Tabulation, Eastern North Pacific Tropical Storms and Hurricanes 1982. E.B. Gunther, June 1983. (PB85 106078)
179 Stratified Maximum Temperature Relationships Between Sixteen Zone Stations in Arizona and Respective Key Stations. Ira S. Brenner, June 1983. (PB83 249904)
180 Standard Hydrologic Exchange Format (SHEF) Version I. Phillip A. Pasteris, Vernon C. Bissel, David G. Bennett, August 1983. (PB85 106052)
181 Quantitative and Spacial Distribution of Winter Precipitation along Utah's Wasatch Front. Lawrence B. Dunn, August 1983. (PB85 106912)
182 500 Millibar Sign Frequency Teleconnection Charts - Winter. Lawrence B. Dunn, December 1983. (PB85 106276)
183 500 Millibar Sign Frequency Teleconnection Charts - Spring. Lawrence B. Dunn, January 1984. (PB85 111367)
184 Collection and Use of Lightning Strike Data in the Western U.S. During Summer 1983. Glenn Rasch and Mark Mathewson, February 1984. (PB85 110534)
185 500 Millibar Sign Frequency Teleconnection Charts - Summer. Lawrence B. Dunn, March 1984. (PB85 111359)

186 Annual Data and Verification Tabulation eastern North Pacific Tropical Storms and Hurricanes 1983. E.B. Gunther, March 1984. (PB85 109635)
187 500 Millibar Sign Frequency Teleconnection Charts - Fall. Lawrence B. Dunn, May 1984. (PB85-110930)
188 The Use and Interpretation of Isentropic Analyses. Jeffrey L. Anderson, October 1984. (PB85-132694)
189 Annual Data & Verification Tabulation Eastern North Pacific Tropical Storms and Hurricanes 1984. E.B. Gunther and R.L. Cross, April 1985. (PB85 1878887AS)
190 Great Salt Lake Effect Snowfall: Some Notes and An Example. David M. Carpenter, October 1985. (PB86 119153/AS)
191 Large Scale Patterns Associated with Major Freeze Episodes in the Agricultural Southwest. Ronald S. Hamilton and Glenn R. Lussky, December 1985. (PB86 144474AS)
192 NWR Voice Synthesis Project: Phase I. Glen W. Sampson, January 1986. (PB86 145604/AS)
193 The MCC - An Overview and Case Study on Its Impact in the Western United States. Glenn R. Lussky, March 1986. (PB86 170651/AS)
194 Annual Data and Verification Tabulation Eastern North Pacific Tropical Storms and Hurricanes 1985. E.B. Gunther and R.L. Cross, March 1986. (PB86 170941/AS)
195 Radid Interpretation Guidelines. Roger G. Pappas, March 1986. (PB86 177680/AS)
196 A Mesoscale Convective Complex Type Storm over the Desert Southwest. Darryl Randerson, April 1986. (PB86 190998/AS)
197 The Effects of Eastern North Pacific Tropical Cyclones on the Southwestern United States. Walter Smith, August 1986. (PB87 106258AS)
198 Preliminary Lightning Climatology Studies for Idaho. Christopher D. Hill, Carl J. Gorski, and Michael C. Conger, April 1987. (PB87 180196/AS)
199 Heavy Rains and Flooding in Montana: A Case for Slantwise Convection. Glenn R. Lussky, April 1987. (PB87 185229/AS)
200 Annual Data and Verification Tabulation Eastern North Pacific Tropical Storms and Hurricanes 1986. Roger L. Cross and Kenneth B. Mielke, September 1987. (PB88 110895/AS)
201 An Inexpensive Solution for the Mass Distribution of Satellite Images. Glen W. Sampson and George Clark, September 1987. (PB88 114038/AS)
202 Annual Data and Verification Tabulation Eastern North Pacific Tropical Storms and Hurricanes 1987. Roger L. Cross and Kenneth B. Mielke, September 1988. (PB88-101935/AS)
203 An Investigation of the 24 September 1986 "Cold Sector" Tornado Outbreak in Northern California. John P. Monteverdi and Scott A. Braun, October 1988. (PB89 121297/AS)
204 Preliminary Analysis of Cloud-To-Ground Lightning in the Vicinity of the Nevada Test Site. Carven Scott, November 1988. (PB89 128649/AS)
205 Forecast Guidelines For Fire Weather and Forecasters -- How Nighttime Humidity Affects Wildland Fuels. David W. Goens, February 1989. (PB89 162549/AS)
206 A Collection of Papers Related to Heavy Precipitation Forecasting. Western Region Headquarters, Scientific Services Division, August 1989. (PB89 230833/AS)
207 The Las Vegas McCarran International Airport Microburst of August 8, 1989. Carven A. Scott, June 1990. (PB90-240268)
208 Meteorological Factors Contributing to the Canyon Creek Fire Blowup, September 6 and 7, 1988. David W. Goens, June 1990. (PB90-245085)
209 Stratus Surge Prediction Along the Central California Coast. Peter Felsch and Woodrow Whitlatch, December 1990. (PB91-129239)
210 Hydrotools. Tom Egger. January 1991. (PB91-151787/AS)
211 A Northern Utah Soaker. Mark E. Struthwolf, February 1991. (PB91-168716)
212 Preliminary Analysis of the San Francisco Rainfall Record: 1849-1990. Jan Null, May 1991. (PB91-208439)
213 Idaho Zone Preformat, Temperature Guidance, and Verification. Mark A. Mollner, July 1991. (PB91-227405/AS)
214 Emergency Operational Meteorological Considerations During an Accidental Release of Hazardous Chemicals. Peter Mueller and Jerry Galt, August 1991. (PB91-235424)
215 WeatherTools. Tom Egger, October 1991. (PB93-184950)
216 Creating MOS Equations for RAWS Stations Using Digital Model Data. Dennis D. Gettman, December 1991. (PB92-131473/AS)
217 Forecasting Heavy Snow Events in Missoula, Montana. Mike Richmond, May 1992. (PB92-196104)
218 NWS Winter Weather Workshop in Portland, Oregon. Various Authors, December 1992. (PB93-146785)
219 A Case Study of the Operational Usefulness of the Sharp Workstation in Forecasting a Mesocyclone-Induced Cold Sector Tornado Event in California. John P. Monteverdi, March 1993. (PB93-178697)
220 Climate of Pendleton, Oregon. Claudia Bell, August 1993. (PB93-227536)
221 Utilization of the Bulk Richardson Number, Helicity and Sounding Modification in the Assessment of the Severe Convective Storms of 3 August 1992. Eric C. Evenson, September 1993. (PB94-131943)
222 Convective and Rotational Parameters Associated with Three Tornado Episodes in Northern and Central California. John P. Monteverdi and John Quadros, September 1993. (PB94-131943)
223 Climate of San Luis Obispo, California. Gary Ryan, February 1994. (PB94-162062)
224 Climate of Wenatchee, Washington. Michael W. McFarland, Roger G. Buckman, and Gregory E. Matzen, March 1994. (PB94-164308)
225 Climate of Santa Barbara, California. Gary Ryan, December 1994. (PB95-173720)
226 Climate of Yakima, Washington. Greg DeVoir, David Hogan, and Jay Neher, December 1994. (PB95-173688)
227 Climate of Kalispell, Montana. Chris Maier, December 1994. (PB95-169488)
228 Forecasting Minimum Temperatures in the Santa Maria Agricultural District. Wilfred Pi and Peter Felsch, December 1994. (PB95-171088)
229 The 10 February 1994 Oroville Tornado--A Case Study. Mike Staudenmaier, Jr., April 1995. (PB95-241873)
230 Santa Ana Winds and the Fire Outbreak of Fall 1993. Ivory Small, June 1995. (PB95-241865)
231 Washington State Tornadoes. Tresté Huse, July 1995. (PB96-107024)
232 Fog Climatology at Spokane, Washington. Paul Frisbie, July 1995. (PB96-106604)
233 Storm Relative Isentropic Motion Associated with Cold Fronts in Northern Utah. Kevin B. Baker, Kathleen A. Hadley, and Lawrence B. Dunn, July 1995. (PB96-106596)
234 Some Climatological and Synoptic Aspects of Severe Weather Development in the Northwestern United States. Eric C. Evenson and Robert H. Johns, October 1995. (PB96-112958)
235 Climate of Las Vegas, Nevada. Paul H. Skrbac and Scott Cordero, December 1995. (PB96-135553)
236 Climate of Astoria, Oregon. Mark A. McInerney, January 1996.
237 The 6 July 1995 Severe Weather Events in the Northwestern United States: Recent Examples of SSWEs. Eric C. Evenson, April 1996.
238 Significant Weather Patterns Affecting West Central Montana. Joe Lester, May 1996. (PB96-178751)
239 Climate of Portland, Oregon. Clinton C. D. Rockey, May 1996. (PB96-17603) - First Revision, October 1999
240 Downslop Winds of Santa Barbara, CA. Gary Ryan, July 1996. (PB96-191697)
241 Operational Applications of the Real-time National Lightning Detection Network Data at the NWSO Tucson, AZ. Darren McCollum, David Bright, Jim Meyer, and John Glueck, September 1996. (PB97-108450)
242 Climate of Pocatello, Idaho. Joe Heim, October 1996. (PB97-114540)
243 Climate of Great Falls. Montana. Matt Jackson and D. C. Williamson, December 1996. (PB97-126684)
244 WSR-88D VAD Wind Profile Data Influenced by Bird Migration over the Southwest United States. Jesus A. Haro, January 1997. (PB97-135263)
245 Climatology of Cape for Eastern Montana and Northern Wyoming. Heath Hockenberry and Keith Meier, January 1997. (PB97-133425)
246 A Western Region Guide to the Eta-29 Model. Mike Staudenmaier, Jr., March 1997. (PB97-144075)
247 The Northeast Nevada Climate Book. Edwin C. Clark, March 1997. (First Revision - January 1998 - Andrew S. Gorelow and Edwin C. Clark - PB98-123250)
248 Climate of Eugene, Oregon. Clinton C. D. Rockey, April 1997. (PB97-155303)
249 Climate of Tucson, Arizona. John R. Glueck, October 1997
250 Northwest Oregon Daily Extremes and Normans. Clinton C. D. Rockey, October 1997
251 A Composite Study Examining Five Heavy Snowfall Patterns for South-Central Montana. Jonathan D. Van Ausdall and Thomas W. Humphrey. February 1998. (PB98-125255)
252 Climate of Eureka, California. Alan H. Puffer. February 1998. (PB98-130735)
253 Inferenced Oceanic Kelvin/Rossby Wave Influence on North American West Coast Precipitation. Martin E. Lee and Dudley Chelton. April 1998. (PB98-139744)
254 Conditional Symmetric Instability--Methods of Operational Diagnosis and Case Study of 23-24 February 1994 Eastern Washington/Oregon Snowstorm. Gregory A. DeVoir. May 1998. (PB98-144660)
255 Creation and Maintenance of a Comprehensive Climate Data Base. Eugene Petrescu. August 1998. (PB98-173529)
256 Climate of San Diego, California. Thomas E. Evans, III and Donald A. Halvorson. October 1998. (PB99-109381)
257 Climate of Seattle, Washington. Dana Felton. November 1998. (PB99-113482)
258 1985-1998 North Pacific Tropical Cyclones Impacting the Southwestern United States and Northern Mexico: An Updated Climatology. Armando L. Garza. January 1999. (PB99-130502)
259 Climate of San Jose, California. Miguel Miller. April 1999. (PB99-145633)
260 Climate of Las Vegas, Nevada. Paul H. Skrbac. December 1999
261 Climate of Los Angeles, California. David Bruno, Gary Ryan, with assistance from Curt Kaplan and Jonathan Slemmer. January 2000
262 Climate of Miles City, Montana. David A. Spector and Mark H. Strobin. April 2000
263 Analysis of Radiosonde Data for Spokane, Washington. Rocco D. Pelatti. November 2000
264 Climate of Billings, Montana. Jeffrey J. Zeltwanger and Mark H. Strobin. November 2000
265 Climate of Sheridan, Wyoming. Jeffrey J. Zeltwanger, Sally Springer, Mark H. Strobin. March 2001

266 Climate of Sacramento, California. Laura Masters-Bevan. December 2000 (7th Revision)
267 Sulphur Mountain Doppler Radar: A Performance Study. Los Angeles/Oxnard WFO. August 2001
268 Prediction of Heavy Snow Events in the Snake River Plain Using Pattern Recognition and Regression Techniques. Thomas Andretta and William Wojcik. October 2003
269 The Lewis and Clark Expedition 18-03-1806, Weather, Water and Climate, Vernon Preston, Pocatello Idaho, December 2004.
270 Climate of San Diego, California, Emmanuel M. Isla, September 2004 (2nd Edition)
271 Climate of Las Vegas, Nevada, Andrew S. Gorelow, January 2005, (2nd Edition)
272 Climate of Sacramento, California, Revised by: Laura A. Bevan and George Cline, June 2005
273 Climate of Flagstaff, AZ 4th Revision. Mike Staudenmaier, Jr, Reginald Preston(R) Paul Sorenson (R) , August 2005
274 Climate of Prescott, AZ, Bob Fogarty, Mike Staudenmaier Jr., Flagstaff WFO, AZ, August 2005.
275 Climate of San Diego, CA, 3rd Revision. Noel M. Isla, Jennifer Lee, March 2006
276 Climate of Reno, NV, Brian Ohara, Reno, NV October 2006
277 Forecaster's Handbook for Extreme Southwestern California Based On Short Term Climatalogical Approximations: Part I - The Marine Layer and Its Effect On Precipitation and Heating Ivory J. Small, October 2006
278 Forecaster's Handbook for Extreme Southwestern California Based On Short Term Climatalogical Approximations: Part II – Wind Effects on Terrestrial and Marine Environments Ivory J. Small, December 2006
279 Effects of Wildfire in the Mountainous Terrain of Southeast Arizona: An Empirical Formula to Estimate 5-Year Peak Discharge from Small Post-Burn Watersheds, William B. Reed and Mike Schaffner , June 2007
280 Climate of Fresno, California, Chris Stachelski, Gary Sanger, February 2008
281 Climate of Bakersfield, California, Chris Stachelski, Gary Sanger, February 2008
282 Hazardous Weather Climatology for Arizona, Craig Shoemaker, Jeffrey T. Davis, February 2008
283 Effects of Wildfire in the Mountainous Terrain of Southeast Arizona: Empirical Formulas to Estimate from 1-Year through 10-Year Peak Discharge from Post-Burn Watersheds, William B. Reed and Mike Schaffner, July 2008

NOAA SCIENTIFIC AND TECHNICAL PUBLICATIONS

The National Oceanic and Atmospheric Administration was established as part of the Department of Commerce on October 3, 1970. The mission responsibilities of NOAA are to assess the socioeconomic impact of natural and technological changes in the environment and to monitor and predict the state of the solid Earth, the oceans and their living resources, the atmosphere, and the space environment of the Earth.

The major components of NOAA regularly produce various types of scientific and technical information in the following kinds of publications.

PROFESSIONAL PAPERS--Important definitive research results, major techniques, and special investigations.

CONTRACT AND GRANT REPORTS--Reports prepared by contractors or grantees under NOAA sponsorship.

ATLAS--Presentation of analyzed data generally in the form of maps showing distribution of rainfall, chemical and physical conditions of oceans and atmosphere, distribution of fishes and marine mammals, ionospheric conditions, etc.

TECHNICAL SERVICE PUBLICATIONS -- Reports containing data, observations, instructions, etc. A partial listing includes data serials; prediction and outlook periodicals; technical manuals, training papers, planning reports, and information serials; and miscellaneous technical publications.

TECHNICAL REPORTS--Journal quality with extensive details, mathematical developments, or data listings.

TECHNICAL MEMORANDUMS--Reports of preliminary, partial, or negative research or technology results, interim instructions, and the like.

Information on availability of NOAA publications can be obtained from:
NATIONAL TECHNICAL INFORMATION SERVICE
U. S. DEPARTMENT OF COMMERCE
5285 PORT ROYAL ROAD
SPRINGFIELD, VA 22161